RICE UNIVERSITY

A CHROMATOGRAPHIC STUDY OF THE OXYGEN EXCHANGE REACTION BETWEEN CARBON MONOXIDE AND CARBON DIOXIDE OVER A Cu-ZnO CATALYST

by

WILLIAM DAVID SMITH

A THESIS SUBMITTED
IN PARTIAL FULFILLMENT OF THE
REQUIREMENTS FOR THE DEGREE OF

DOCTOR OF PHILOSOPHY IN CHEMICAL ENGINEERING

Thesis Director's Signature:

Houston, Texas

June, 1972

ABSTRACT

A CHROMATOGRAPHIC STUDY OF THE OXYGEN EXCHANGE REACTION BETWEEN CARBON MONOXIDE AND CARBON DIOXIDE OVER A Cu-ZnO CATALYST

by

William David Smith

Perturbation chromatography and, more specifically, the use of isotopic tracers have been applied successfully to the investigation of equilibrium and nonequilibrium chemisorption and surface reaction in a gas-solid system.

The theoretical treatment of the problem resulted in equations describing the movement of tracer samples down a packed column when adsorption and reaction processes were at equilibrium. In general, the assumption that these processes were near equilibrium was not valid. In order to describe the data over the entire range of flow rates, it was necessary to solve the continuity equations numerically.

The experimental system consisted of carbon monoxide and carbon dioxide, along with their carbon-14 isotopes, in the presence of a copper-zinc oxide catalyst at 400°F. The catalyst, Girdler G-66B, is a commercial low temperature

water gas shift catalyst.

A five step adsorption-reaction mechanism was found to fit the data very well. Simpler mechanisms were attempted and found to be qualitatively unsatisfactory. The mechanism assumes two different types of adsorption for both carbon monoxide and carbon dioxide. In each case only one form of adsorption is directly involved in the exchange reaction. The mechanism is not specific regarding the nature of the oxygen exchange on the surface.

A brief investigation of the carbon dioxide - helium system showed that carbon dioxide adsorption on this catalyst follows a Freundlich isotherm at 400°F. The existence of dissociative carbon dioxide adsorption was neither proven nor disproven.

The absence of Langmuir behavior in both systems leads to the conclusion that the surface of this catalyst is extremely heterogeneous energetically.

ACKNOWLEDGEMENTS

The author would like to express his appreciation and gratitude to the following persons and organizations:

Dr. H. A. Deans - for his assistance and guidance as principal advisor.

Dr. L. V. McIntire and Dr. R. L. Sass - for serving on the thesis committee.

Dr. Claude R. Hocott and the Esso Production Research Company - for providing the computer time.

Mr. L. Guzman and the Chemetron Corporation - for supplying the catalyst.

Dr. J. W. Hightower - for use of the mass spectrometer and the vacuum system.

Dr. W. R. Cares and Dr. W. R. Murphy - for assistance in the mass spectral analysis.

Mr. S. E. Riffle - for assistance in troubleshooting the equipment.

The National Science Foundation, the National Defense Education Act, and Rice University - for financial support.

TABLE OF CONTENTS

LIST OF TABLES

LIST OF FIGURES

TABLE OF NOMENCLATURE

Capital Letters

A	Concentration of unoccupied type "A" surface sites, moles/mole flowing phase
A_B	Bypass peak area
A_C	Column peak area
A_z	Concentration of type "A" surface sites, moles/mole flowing phase
B	Concentration of unoccupied type "B" surface sites, moles/mole flowing phase
B_z	Concentration of type "B" surface sites, moles/mole flowing phase
C	Concentration of unoccupied type "C" surface sites, moles/mole flowing phase
C_s	Chart speed for long column operation
C_{s1}	Chart speed for short column operation, column peak
C_{s2}	Chart speed for short column operation, bypass peak
C_z	Concentration of type "C" surface sites, moles/mole flowing phase

D	Flowing phase dispersion coefficient
F^*	Rate of the isotopic exchange reaction
F_k	Rate of surface reaction "k"
G^*	Retention product defined in equation (II-14)
K	Equilibrium constant for the exchange reaction
K'	Equilibrium function for the exchange reaction, defined in equation (II-29)
K_ℓ	Equilibrium constant for step "ℓ" in the mechanism
K_4'	Equilibrium function for the surface reaction in the mechanism, mole B type CO/mole B type CO_2
L_r	Chart length between bypass and main peaks
L_{r1}	Chart length between main peak and injection
L_{r2}	Chart length between bypass peak and injection
N	Number of tanks used to model the column
P_a	Barometric pressure
P_c	Average column pressure
P_{H_2O}	Vapor pressure of water at room temperature
P_i	Column inlet pressure
P_o	Column outlet pressure
Q	Carrier gas flow rate, column conditions
Q_m	Carrier gas flow rate measured by soap bubble meter
R	Gas constant in ideal gas law
R_i	Source term for component "i" in the flowing phase

R_i'	Source term for component "i" in the flowing phase, $R_i' = R_i/c$
$\overline{R}_i$	Source term for component "i" in the stationary phase
T_c	Column temperature
T_r	Room temperature
V_G	Column free volume
V_t	Tank volume, $V_t = V_G/N$

Small Letters

a	Constant in Langmuir isotherm expressions
b	Constant in Langmuir isotherm expressions
c	Total molar concentration of the flowing phase
c_i	Molar concentration of component "i" in the flowing phase
d	Constant in Freundlich isotherm expression
f	Constant in Freundlich isotherm expression
f_B	Fraction of flow through bypass
j	Index used to identify each tank in column model
k_ℓ	Rate constant for step "ℓ" in the mechanism
k_ℓ'	Rate constant for step "ℓ", $k_\ell' = k_\ell \cdot$ (A, B, or C)
m	Mass of catalyst in the column
n	Number of components in carrier gas
n_i	Surface concentration of component "i", moles i/mole flowing phase

n_i'	Surface concentration of component "i", moles i/g catalyst
n_i^M	Surface concentration of component "i" on site "M", moles i/mole flowing phase
r_ℓ	Rate for step "ℓ" in the mechanism
t	Time
t_p	Peak residence time
t_r	Carrier gas residence time
$\bar{u}$	Flowing phase velocity vector
v	Average velocity of flowing phase
v_c	Characteristic velocity of mass perturbation
v_c^*	Characteristic velocity of tracer
y_i	Flowing phase mole fraction of component "i"
z	Axial distance

Greek Letters

β	Column conversion constant, $\frac{m}{V_G\ c}$
μ_i	Adsorption equilibrium function for component "i", mole i on surface/mole i flowing phase
μ_i'	Adsorption equilibrium function for component "i", $\mu_i' = \mu_i/\beta$
μ_i^M	Adsorption equilibrium function for component "i" on site "M"

$\mu_i^{M'}$	Adsorption equilibrium function for component "i" on site "M", $\mu_i^{M'} = \mu_i^M/\beta$
ν_{ik}	Stoichiometric coefficient for component "i" for the kth surface reaction
τ	Dimensionless time

Subscripts

i	Component "i"
k	Reaction "k"
ℓ	Step "ℓ" in the mechanism
M	Adsorption site "M"

Superscripts

s	Steady state
*	Radioactive component

I. INTRODUCTION AND LITERATURE REVIEW

I.1 Introduction

In the past chemisorption of gases on catalytic surfaces has been studied most often in static systems. In the past decade, however, perturbation chromatography and the use of distinguishable molecular pulses (tracers) has emerged as a valuable new approach in chemisorption studies.

In this work, the theory and practice of perturbation chromatography and the use of radioactive tracers has been applied to the investigation of carbon monoxide and carbon dioxide adsorption on a copper-zinc oxide surface. The solid used was Girdler G-66B, a commercial low temperature water gas shift catalyst.

The purpose of this work was twofold. First, it was desired to extend the application of perturbation chromatography to the study of chemisorption in the presence of a surface reaction. Second, it was hoped that some contribution might be made to the fundamental understanding of carbon monoxide and carbon dioxide chemisorption over this catalyst.

The use of radioactive tracers eliminated any restrictions regarding the linearity of adsorption isotherms. Information was not extracted from mass peaks, which also

result when tracer samples are injected, primarily because of poor detector sensitivity. The theory which is presented to account for the phenomena observed yielded sparingly to analytical solution. Most of the comparison between theory and experiment was accomplished by numerical solution of the equations resulting when the column was simulated by a series of perfectly mixed tanks.

I.2 Literature Review

Chromatography was introduced to the world in 1906 by Tswett (53), who used the procedure to separate plant pigments. The column effluent consisted of several zones of different colors, due to the pigments, and as a result Tswett coined the word chromatography, which means "color-writing," to describe the process. Evidently his work went somewhat unheralded, for it was not until 1941 when the next work in chromatography was published. Martin and Synge (37) introduced the plate theory to partition chromatography and applied it to a liquid-liquid system. James and Martin (25) used a gas as a carrier and thus initiated work in the field of gas chromatography. As the research effort in chromatography began to accelerate, Littlewood et al. (35) used chromatography to calculate heats of solution. Martin (36) suggested the use of gas-liquid partition

chromatography to determine thermodynamic quantities such as interaction potentials.

A number of reviews have been written about chromatography (22, 26, 27, 29, 42). Purnell (42), along with Keulemans (27), was concerned primarily with separation chromatography while Kobayashi et al. (29) concentrated on the use of chromatography in physico-chemical measurements.

Since the mid-1950's a voluminous amount of work has been conducted in chromatography. Most of the work has been concerned with retention volumes or retention times. Stalkup and Kobayashi (47), by measuring retention volumes, determined K values for n-butane in methane-n-decane at high pressure. Stalkup and Kobayashi (46) in a later work confirmed the theory presented in a paper by Stalkup and Deans (45) which predicted N-1 peak velocities for an N component flowing phase infinitesimally perturbed. Koonce et al. (30) demonstrated that a radioactive peak has a different velocity than the concentration peak. Barrere and Deans (4) used chromatography to study absorption with chemical reaction in the carbon dioxide-diethanolamine system. Eberly (11) applied gas-solid chromatography to the measurement of adsorption isotherms, surface areas, and heats of adsorption at high temperatures.

In a classic paper which stirred interest in peak shape, Van Deemter et al. (55) introduced a relationship

between zone spreading and plate height, which, unfortunately, could not be used a priori to calculate plate height. Giddings (19) introduced the concept of generalized diffusion coefficients which included the kinetic constants of the rate processes involved. Giddings and Seager (21) pointed out that the total variance of a peak could be expressed as the sum of the variances of a number of independent processes. Giddings and Keller (20) qualitatively discussed a slow reversible first order unimolecular reaction under chromatographic conditions for no reaction, intermediate reaction, and complete reaction cases. Klinkenberg (28) analyzed this reaction in a chromatographic column for the latter case and expressed the results in terms of retention time and zone spreading. Kubin (31) and Kucera (33) used LaPlace transforms in solving for expressions for the moments of the eluted peak in gas-solid chromatographic systems. Smith and co-workers (41, 43, 44, 49) combined their results with experimental first and second moments to determine adsorption isotherms, adsorption rate constants, intraparticle diffusion coefficients, surface diffusion coefficients, and axial dispersion coefficients. Aris (2) introduced the moment method, in which the axial distance variable is transformed, by using it to solve the problem of dispersion in capillary flow originally solved by Taylor (50). The moment method has since been used by

Deans et al. (9) to develop a generalized theory of perturbation chromatography in multicomponent systems involving an arbitrary number of chemical reactions. Recently Gangwal et al. (16) applied Fourier analysis to chromatographic peaks.

Carbon monoxide has been observed to adsorb on many solids (1, 5, 12, 13, 14, 15, 17, 18, 24, 32, 34, 39, 51, 58). Eischens and Webb (13) observed the dissociation of carbon monoxide over an iron catalyst, and Ertl (15) observed carbon formation in the carbon monoxide - copper system at high temperatures. Most other work (5, 12, 14) has shown carbon monoxide chemisorption not to be dissociative. Carbon dioxide adsorption in general is not as extensive as that of the monoxide. Unlike the monoxide, carbon dioxide adsorbs both associatively (18, 23, 24, 39, 58) and dissociatively (7, 23, 58). Both carbon oxides have been found to adsorb reversibly on zinc oxide at room temperature (1, 17, 18, 32, 51, 56). Infrared studies (1, 51) on zinc oxide indicated that there exists more than one type of carbon monoxide chemisorption and that surface carbon dioxide exists primarily as a carbonate type structure. Nekipelov and Kasatkina (39) noted that dissociative carbon dioxide adsorption did not occur on their zinc oxide catalyst and were in agreement with Winter (56) in concluding

that the oxygen exchange reaction between carbon monoxide and carbon dioxide was negligible over zinc oxide.

Oxygen exchange between both carbon oxides and catalyst oxygen has been observed over both zinc oxide and cuprous oxides (24, 39, 52). Several investigators (3, 7, 39, 40, 48, 56) have conducted kinetic studies of the oxygen exchange reaction,

$$C^*O + C\,O_2 \rightleftarrows C^*O_2 + C\,O$$

where the * denotes a nonnormal carbon isotope, such as carbon-14. Stroeva et al. (48) measured rate constants for this reaction in the presence of iron oxide, copper, silver, platinum, and cobalt. In spite of the fact that carbon dioxide adsorption on copper oxide at low temperatures is negligible (24, 57), copper was found to catalyze the oxygen exchange reaction in the 250°C - 400°C temperature range. Following the kinetic experiments X-ray analysis of the catalyst indicated that very little of the copper was present as oxide. Cha and Parravano (7) observed this reaction over a titanium dioxide catalyst and concluded that carbon dioxide adsorption was rate limiting.

The copper-zinc oxide catalyst (G-66B) employed in this work was a commercial low temperature shift catalyst. It is generally thought that the catalytic activity for the

water gas shift reaction is provided by the copper, with the zinc oxide playing the role of a support and a spacer to inhibit thermal sintering of the finely dispersed copper (6). Uchida et al. (54) investigated similar copper-zinc oxide catalysts by X-ray and electron microscope techniques. They found the copper to exist primarily in the metallic state and to be of two general types according to structure: (1) large massive particles several hundred Å in size, and (2) thin patches covering the zinc oxide surface. Musser (38) showed that carbon monoxide chemisorption on G-66B was not due exclusively to a one site mechanism, although he was unable to differentiate between various two site mechanisms. A chromatographic study of hydrogen chemisorption was carried out on this catalyst by Suzuki and Smith (49). Their work yielded good adsorption data but no conclusions were reached regarding the mechanism involved.

II. THEORY

II.1 General Description

The transient behavior of a slug of tracer being swept down a packed column by a multicomponent carrier gas is to be described. It is assumed that the tracer adsorbs on the surface of the catalyst and may react while on the surface of the catalyst to become a different chemical component. The general mass balance for the tracer in the flowing phase may be written as follows:

$$\frac{\partial c_i}{\partial t} + \nabla \cdot c_i \bar{u} = \nabla \cdot D\nabla c_i + R_i \qquad \text{(II-1)}$$

where: $\bar{u}$ = flowing phase velocity vector

c_i = concentration of component "i"

D = dispersion coefficient

R_i = source of component "i" in the flowing phase

Equation (II-1) can be simplified by introduction of the following assumptions:

(1) Flow is in the axial direction only.

(2) Flowing phase dispersion is negligible, and therefore $D = 0$.

The simplified form is

$$\frac{\partial c_i}{\partial t} + v \frac{\partial c_i}{\partial z} + c_i \frac{\partial v}{\partial z} = R_i \qquad \text{(II-2)}$$

where: v = average fluid velocity

Collins (8) has shown that for the system to which this theoretical treatment will be applied, injection of a tracer component also results in a concentration disturbance which propagates down the column at a velocity different from that of the tracer. At all points upstream and downstream of this perturbation the total concentration of each chemical component in the carrier gas remains constant at the steady state value that was established before injection of the sample. This is illustrated for a two component system in Figure II-1. Furthermore, Collins' analysis pointed out that the term $\frac{\partial v}{\partial z}$ was zero except for certain cases in the region of the perturbation. Therefore, since the tracer will not be at the same location as the concentration perturbation, the term $\frac{\partial v}{\partial z}$ can be set equal to zero, and the analysis can be simplified a great deal.

At this point the following assumptions are to be made:

(3) The pressure drop across the column is negligible, so that the pressure can be assumed constant.

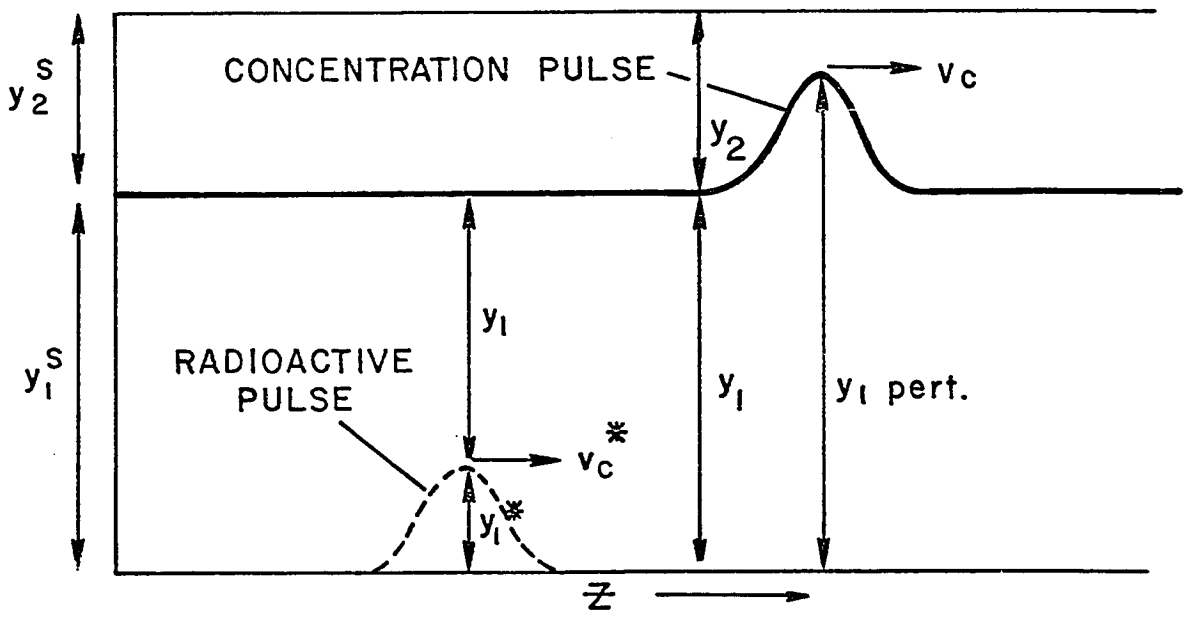

FIGURE II-1 CHARACTERISTIC VELOCITIES

(4) The column is isothermal.

(5) The flowing phase is an ideal gas mixture.

Introducing these assumptions and setting $\frac{\partial v}{\partial z}$ equal to zero transforms equation (II-2) as follows:

$$\frac{\partial y_i}{\partial t} + v \frac{\partial y_i}{\partial z} = R_i' \qquad \text{(II-3)}$$

where: y_i = mole fraction of component "i" in the following phase

$R_i' = R_i/c$

c = total molar concentration of the flowing phase

II.2 Equilibrium Theory

II.2.1 Generalization

At this point the following assumptions are made:

(6) All mass transfer and adsorption rates are infinitely fast; i.e., local equilibrium exists.

(7) Any reactions occurring on the surface are reversible and at equilibrium.

The material balance in the stationary phase is

$$\frac{\partial n_i}{\partial t} = \overline{R}_i \qquad \text{(II-4)}$$

where: n_i = surface concentration of component "i", moles "i"/mole flowing phase

$\overline{R}_i$ = source of component "i" in the stationary phase

Incorporating assumptions 6 and 7 leads to the following relationship:

$$\overline{R}_i = -R_i' + \sum_k \nu_{ik} F_k \qquad \text{(II-5)}$$

where: F_k = rate of the kth surface reaction

ν_{ik} = the stoichiometric coefficient of component "i" in the kth surface reaction

At this point it becomes necessary to introduce a relationship for the equilibrium existing between the two phases. Such a relation is

$$n_i = \mu_i y_i \qquad \text{(II-6)}$$

where: μ_i = the adsorption equilibrium function of component "i", moles "i" on the surface/mole "i" in the flowing phase and $\mu_i = \mu_i(T_c, P_c, y_1, y_2, y_3, \ldots y_{n-1}$, catalyst, etc.)

where: T_c = column temperature

P_c = column pressure

y_i = mole fraction component "i" in the flowing phase

n = number of components in the carrier gas

The equilibrium function, μ_i, can be treated as a constant, since by assumption P_c and T_c are constant and in the vicinity of the tracer peak the total concentrations of distinguishable chemical species are constant.

Combining equations (II-3) through (II-6) yields

$$\frac{\partial y_i}{\partial t} + v \frac{\partial y_i}{\partial z} + \left(\mu_i \frac{\partial y_i}{\partial t} - \sum_k \nu_{ik} F_k\right) = 0 \qquad \text{(II-7)}$$

II.2.2 Adsorption Without Reaction

Consider a binary carrier gas consisting of components A and B. Equation (II-7) can be applied to describe the behavior of a tracer component, A*, which is assumed to be chemically indistinguishable from component A. In this case, since it has been assumed that there is no surface reaction, $F_k = 0$. Equation (II-7) becomes for the A-B-A* system, where 1 and 2 represent components A and B, respectively,

$$(1 + \mu_1) \frac{\partial y_1^*}{\partial t} + v \frac{\partial y_1^*}{\partial z} = 0 \qquad \text{(II-8)}$$

where: y_i^* denotes the isotopic tracer "i".

Equation (II-8), being a hyperbolic partial differential equation, can be solved by the method of characteristics. This method has been well documented with respect to chromatographic systems (4, 8, 38). The characteristic velocity, v_c^*, is given by

$$v_c^* = \left(\frac{\partial z}{\partial t} \right)_{y_i^*} \qquad \text{(II-9a)}$$

or

$$v_c^* = -\left(\frac{\partial y_i^*}{\partial t} \right) / \left(\frac{\partial y_i^*}{\partial z} \right) \qquad \text{(II-9b)}$$

The solution of equation (II-8), therefore, is

$$v_c^* = \frac{v}{1 + \mu_1} \qquad \text{(II-10)}$$

This can be rearranged to give

$$\mu_1 = \left(\frac{v}{v_c^*} - 1 \right) \qquad \text{(II-11)}$$

In terms of more readily obtainable experimental quantities equation (II-11) becomes

$$\mu_1 = \left(\frac{t_p}{t_r} - 1 \right) \qquad \text{(II-12)}$$

where: t_p = residence of the peak

t_r = residence time of the carrier gas

A column conversion constant, β, can be defined as follows:

$$\beta = \frac{m}{V_G c} \tag{II-13}$$

where: m = mass of catalyst in the column

V_G = column free volume

Dividing equation (II-12) by β gives the experimental quantity G*, which is given in the following equation:

$$G^* = \frac{1}{\beta} \left(\frac{t_p}{t_r} - 1 \right) \tag{II-14}$$

and by equation (II-12)

$$G^* = \mu_1' \tag{II-15}$$

where: $n_i' = \mu_i' y_i$ (II-16)

and n_i' = moles of component "i"/g catalyst

μ_i' = adsorption equilibrium function of component "i", $\mu_i' = \mu_i/\beta$

Now consider the addition of a second tracer component, B*. A four component system, A-B-A*-B*, now exists and a second equation appears as

$$(1 + \mu_2) \frac{\partial y_2^*}{\partial t} + v \frac{\partial y_2^*}{\partial z} = 0 \tag{II-17}$$

Since there is no surface reaction ($F_k = 0$) equations (II-8) and (II-17) are not coupled, and each can be solved separately by the method of characteristics. The solution to equation (II-17) is

$$G^* = \mu_2' \qquad \text{(II-18)}$$

II.2.3 Equilibrium Reaction

Now consider the case of the four component system, A-B-A*-B*, under conditions in which the following reaction may be assumed at equilibrium:

$$A + B^* \rightleftarrows B + A^*$$

$$y_1\ y_2^* \qquad y_2\ y_1^*$$

where: y_i = flowing phase mole fraction of component "i"
y_i^* = flowing phase mole fraction of isotopic tracer of "i"

The presence of the above exchange reaction reduces the degrees of freedom for the system from two to one. Because of the coupling effect of the reaction, both tracer components will have the same characteristic velocity as opposed to the case described in Section II.2.2. For the tracer components, equation (II-7) becomes

$$\frac{\partial y_1^*}{\partial t} + v \frac{\partial y_1^*}{\partial z} + \mu_1 \frac{\partial y_1^*}{\partial t} - F^* = 0 \qquad \text{(II-19a)}$$

$$\frac{\partial y_2^*}{\partial t} + v \frac{\partial y_2^*}{\partial z} + \mu_2 \frac{\partial y_2^*}{\partial t} + F^* = 0 \qquad \text{(II-19b)}$$

where: F^* = the rate of the exchange reaction

The form of the equilibrium constant for the exchange reaction is assumed to be

$$K = \frac{y_1^* y_2}{y_2^* y_1} \qquad \text{(II-20a)}$$

or

$$\frac{y_1^*}{y_2^*} = K \frac{y_1}{y_2} \qquad \text{(II-20b)}$$

Combining equation (II-20b) with

$$y_i^s = y_i^* + y_i \qquad \text{(II-21)}$$

where: y_i^s = the steady state mole fraction of component "i" yields

$$\frac{y_1^*}{y_2^*} = K \frac{y_1^s}{y_2^s} \qquad \text{(II-22)}$$

That is, in the vicinity of the tracer pulse, the ratio of the tracer components is constant.

With this restriction, equation (II-19a) can be multiplied by $(1/y_1^*)$ and added to the product of equation (II-19b) and $(-1/y_2^*)$ to give

$$F^* = \frac{y_2^* \mu_1 \frac{\partial y_1^*}{\partial t}}{y_1^* + y_2^*} - \frac{y_1^* \mu_2 \frac{\partial y_2^*}{\partial t}}{y_1^* + y_2^*} \qquad \text{(II-23)}$$

Equation (II-23) can be rearranged by using equation (II-22) as follows:

$$F^* = \frac{\mu_1 \frac{\partial y_1^*}{\partial t}}{1 + \frac{K\, y_1^s}{y_2^s}} - \frac{\mu_2 \frac{\partial y_2^*}{\partial t}}{1 + \frac{y_2^s}{K\, y_1^s}} \qquad \text{(II-24)}$$

Substitution of equation (II-24) into equation (II-19a) results in

$$\frac{\partial y_1^*}{\partial t} + v \frac{\partial y_1^*}{\partial z} + \frac{K\mu_1\, y_1^s \frac{\partial y_1^*}{\partial t}}{y_2^s + K\, y_1^s} + \frac{K\, y_1^s\, \mu_2 \frac{\partial y_2^*}{\partial t}}{K_1\, y_1^s + y_2^s} = 0 \qquad \text{(II-25)}$$

Using equation (II-22) to convert the last term of equation (II-25) gives

$$\frac{\partial y_1^*}{\partial t}\left(1 + \frac{K\mu_1 y_1^s + \mu_2 y_2^s}{K y_1^s + y_2^s}\right) + v\frac{\partial y_1^*}{\partial z} = 0 \qquad \text{(II-26)}$$

Once again solving by the method of characteristics gives as the solution to equation (II-26)

$$G^* = \frac{K\mu_1' y_1^s + \mu_2' y_2^s}{K y_1^s + y_2^s} \qquad \text{(II-27)}$$

The addition, then, of an equilibrium reaction in the four component system, A-B-A*-B*, results in reducing the number of tracer peaks from two to one, with the subsequent value of G* resulting in a linear combination of the G* values to be expected when there is no reaction.

II.3 Nonequilibrium Theory

In Section II.2 equation (II-3) was applied to cases in which all adsorption and reaction rate processes were either sufficiently rapid to be assumed at equilibrium or slow enough to be neglected. At the intermediate stages, where neither of these assumptions is valid, the equations can no longer be put in the hyperbolic form. The equations can be solved numerically, however, by simulating the column by a series of perfectly mixed tanks according to the method

of Deans and Lapidus (10).

As explained in Section II.2.3 the coupling is provided by the exchange reaction. If the isotopic tracers are assumed to be infinitely dilute, the mole fractions of A and B can be assumed to be constant and equal to the steady state mole fractions. The exchange reaction can then effectively be written as

$$\underset{y_2^*}{B^*} \rightleftarrows \underset{y_1^*}{A^*}$$

Following equation (II-20a), the equilibrium can be expressed as

$$\left(\frac{y_1^*}{y_2^*} \right) = K' \qquad \text{(II-28)}$$

where: $$K' = K \frac{y_1^s}{y_2^s} \qquad \text{(II-29)}$$

In general it must be assumed that both adsorption and reaction processes may not be at equilibrium. In such a case the two tracer components can be described by equation (II-3) as follows:

$$\frac{\partial y_1^*}{\partial t} + v \frac{\partial y_1^*}{\partial z} - R_1'^* = 0 \qquad \text{(II-30a)}$$

$$\frac{\partial y_2^*}{\partial t} + v \frac{\partial y_2^*}{\partial z} - R_2'^* = 0 \qquad \text{(II-30b)}$$

Equations (II-30) could be placed in the form of equation (II-7) if it could be assumed that all the adsorption processes were at equilibrium.

The exact form of $R_1'^*$ and $R_2'^*$ depends on the mechanism chosen to explain the adsorption and reaction phenomena. Equations (II-30) can be rewritten for each tank "j" used in modeling the column as follows:

$$\frac{d\, y_1^*(j)}{d\tau} = y_1^*(j-1) - y_1^*(j) + \frac{V_t\, R_1'^*(j)}{Q} \qquad \text{(II-31a)}$$

$$\frac{d\, y_2^*(j)}{d\tau} = y_2^*(j-1) - y_2^*(j) + \frac{V_t\, R_2'^*(j)}{Q} \qquad \text{(II-31b)}$$

where: $\tau = \frac{t\, Q}{V_t}$ (II-32)

and $V_t = V_G/N$ (II-33)

where: Q = column flow rate

V_t = volume of each tank

N = number of tanks used to simulate the column

II.4 The CO - CO_2 - $C^{14}O$ - $C^{14}O_2$ System

II.4.1 General

An interesting practical example of the theoretical three and four component systems discussed in Sections II.2 and II.3 is the mixture consisting of carbon monoxide and carbon dioxide and one or both of their respective carbon-14 isotopes in the presence of a Cu-ZnO water gas shift catalyst. The impetus to investigate this system stems from the fact that the catalyst is commercial and in common usage. It is of interest therefore to attempt to understand the surface chemistry involved with this catalyst and the carbon oxides, which are two of the four major chemical species involved in the water gas shift reaction. Musser (38) has investigated carbon monoxide adsorption and the oxygen exchange reaction between carbon monoxide and carbon dioxide over this catalyst. The oxygen exchange reaction can be written as

$$\underset{y_1}{CO} + \underset{y_2^*}{C^{14}O_2} \rightleftarrows \underset{y_1^*}{C^{14}O} + \underset{y_2}{CO_2}$$

Musser found that by varying the flow rate the extent of the exchange reaction could be controlled.

For high flow rates in a short column, it might reasonably be assumed that the exchange reaction is negligible. Under such conditions, the retention of each tracer may be expressed according to equations (II-15) and (II-18) as follows:

$$G^* = \mu'_{CO} \tag{II-34a}$$

$$G^* = \mu'_{CO_2} \tag{II-34b}$$

For the opposite situation, in which there are low flow rates in long columns, it is assumed that the exchange reaction is at equilibrium. It is further assumed that the equilibrium constant, K, for this reaction is equal to unity. According to equation (II-27), then, and using the fact that $\sum_i y_i = 1$, the relationship for G* is

$$G^* = \mu'_{CO}\, y^s_{CO} + \mu'_{CO_2}\, y^s_{CO_2} \tag{II-35}$$

II.4.2 The Mechanism

Musser (38), in his brief look at this reaction, attempted unsuccessfully to explain his data in terms of a single surface reaction coupling two surface species. The mechanism shown on the following page was advanced to explain the reaction and adsorption phenomena observed on

this catalyst. Since dissociative adsorption on metals is not uncommon (24), it was assumed that a dissociative carbon dioxide adsorption step was the key to the exchange reaction. The basis for assuming this five step mechanism is presented in Section IV.1.2.

1. $CO + A \rightleftarrows \underset{A}{CO}$

2. $CO + B \rightleftarrows \underset{B}{CO}$

3. $CO_2 + B \rightleftarrows \underset{B}{CO_2}$

4. $\underset{B}{CO_2} + B \rightleftarrows \underset{B}{CO} + \underset{B}{O}$

5. $CO_2 + C \rightleftarrows \underset{C}{CO_2}$

The assumed equilibrium relationships are as follows:

$$K_1 = \frac{n^A_{CO}}{y_{CO}\ A} \qquad \text{(II-36a)}$$

$$K_2 = \frac{n^B_{CO}}{y_{CO}{}^B} \qquad \text{(II-36b)}$$

$$K_3 = \frac{n^B_{CO_2}}{y_{CO_2}\ B} \qquad \text{(II-36c)}$$

$$K_4 = \frac{n^B_{CO}\, n^B_0}{n^B_{CO_2}\, B} \qquad \text{(II-36d)}$$

$$K_5 = \frac{n^C_{CO_2}}{y_{CO_2}\, C} \qquad \text{(II-36e)}$$

where: n^M_i = surface concentration of component "i" on site "M"

A,B,C = concentration of unoccupied type A, B, C, adsorption sites, respectively, moles of site/mole flowing phase

and $$A = \frac{A_z}{1 + K_1\, y_{CO}} \qquad \text{(II-37a)}$$

$$B = \frac{B_z}{1 + K_2\, y_{CO} + K_3\, y_{CO_2} + \frac{K_3\, K_4}{K_2}\, \frac{y_{CO_2}}{y_{CO}}} \qquad \text{(II-37b)}$$

$$C = \frac{C_z}{1 + K_5\, y_{CO_2}} \qquad \text{(II-37c)}$$

where: A_z, B_z, C_z = total site concentrations of type A, B, C, respectively, mole site/mole flowing phase

It should be pointed out that since in the vicinity of the tracer the total concentration of each distinguishable chemical component is constant, the quantities A, B, C and n_0^B are constant for a given carrier gas.

Equations (II-36) can be placed in the form of equation (II-6) as follows:

$$\mu_{CO}^{A} = n_{CO}^{A}/y_{CO} \qquad \text{(II-38a)}$$

$$\mu_{CO}^{B} = n_{CO}^{B}/y_{CO} \qquad \text{(II-38b)}$$

$$\mu_{CO_2}^{B} = n_{CO_2}^{B}/y_{CO_2} \qquad \text{(II-38c)}$$

$$K_4' = n_{CO}^{B}/n_{CO_2}^{B} \qquad \text{(II-38d)}$$

$$\mu_{CO_2}^{C} = n_{CO_2}^{C}/y_{CO_2} \qquad \text{(II-38e)}$$

where: μ_i^M = the adsorption equilibrium function of component "i" on site "M"

K_4' = surface chemical equilibrium function, mole B type CO/mole B type CO_2

II.4. Application of the Equilibrium Theory

Since the mechanism proposes two types of adsorption

for carbon monoxide, the following expression can be written:

$$n_{CO} = n_{CO}^{A} + n_{CO}^{B} \qquad \text{(II-39a)}$$

and, therefore

$$\mu_{CO} = \mu_{CO}^{A} + \mu_{CO}^{B} \qquad \text{(II-39b)}$$

Equation (II-34a) describes the situation in which both types of adsorption are near equilibrium. Now consider the case in which type B carbon monoxide adsorption is negligibly slow. In this case equation (II-15) becomes

$$G^* = \mu_{CO}^{A'} \qquad \text{(II-40)}$$

Similarly, for the carbon dioxide, assuming step 3 to always be rapid while step 5 is negligible, equation (II-18) becomes

$$G^* = \mu_{CO_2}^{B'} \qquad \text{(II-41)}$$

Accordingly, there are two subcases when the exchange reaction is at equilibrium, depending on whether or not step 5 is included. If this carbon dioxide adsorption step can be neglected, equation (II-35) is modified to

become

$$G^* = \mu'_{CO}\, y^s_{CO} + \mu^{B'}_{CO_2}\, y^s_{CO_2} \qquad \text{(II-42)}$$

On the other hand, if all five steps of this mechanism can be assumed to be near equilibrium, equation (II-35) remains unchanged.

$$G^* = \mu'_{CO}\, y^s_{CO} + \mu'_{CO_2}\, y^s_{CO_2} \qquad \text{(II-35)}$$

II.4.4 The Nonequilibrium Treatment

For the regions in which nonequilibrium processes cannot be neglected, the coupled equations can be solved numerically as explained in Section II.3. The rate equations for the five steps are as follows:

$$r_1 = k_1\, A(y^*_{CO} - n^{A*}_{CO}/\mu^A_{CO}) \qquad \text{(II-43a)}$$

$$r_2 = k_2\, B(y^*_{CO} - n^{B*}_{CO}/\mu^B_{CO}) \qquad \text{(II-43b)}$$

$$r_3 = k_3\, B(y^*_{CO_2} - n^{B*}_{CO_2}/\mu^B_{CO_2}) \qquad \text{(II-43c)}$$

$$r_4 = k_4\, B(n^{B*}_{CO_2} - n^{B*}_{CO}/K'_4) \qquad \text{(II-43d)}$$

$$r_5 = k_5\, C(y^*_{CO_2} - n^{C*}_{CO_2}/\mu^{C}_{CO_2}) \qquad \text{(II-43e)}$$

where: r_ℓ = rate of step "ℓ", dimensionless

k_ℓ = rate constant of step "ℓ", dimensionless

The source terms, $\frac{V_t\, R_1'^*(j)}{Q}$ and $\frac{V_t\, R_2'^*(j)}{Q}$, in equations (II-31) can now be expressed as follows:

$$\frac{V_t\, R_1'^*(j)}{Q} = -\, r_1(j) - r_2(j) \qquad \text{(II-44a)}$$

$$\frac{V_t\, R_2'^*(j)}{Q} = -\, r_3(j) - r_5(j) \qquad \text{(II-44b)}$$

Equations (II-31) now become

$$\frac{d\, Y^*_{CO}(j)}{d\tau} = y^*_{CO}(j-1) - y^*_{CO}(j) - r_1(j) - r_2(j) \qquad \text{(II-45a)}$$

$$\frac{d\, y^*_{CO_2}(j)}{d\tau} = y^*_{CO_2}(j-1) - y^*_{CO_2}(j) - r_3(j) - r_5(j) \qquad \text{(II-45b)}$$

The rate equations for the four surface species are

$$\frac{d\, n^{A*}_{CO}}{d\tau} = r_1(j) \qquad \text{(II-46a)}$$

$$\frac{d\, n^{B*}_{CO}}{d\tau} = r_2(j) + r_4(j) \qquad \text{(II-46b)}$$

$$\frac{d\, n_{CO_2}^{B*}}{d\tau} = r_3(j) - r_4(j) \qquad \text{(II-46c)}$$

$$\frac{d\, n_{CO_2}^{C*}}{d\tau} = r_5(j) \qquad \text{(II-46d)}$$

III. EXPERIMENTAL

III.1 Equipment

The equipment, along with the direction of gas flow, is depicted schematically in Figure III-1. Carbon monoxide-carbon dioxide and helium-carbon dioxide carrier gas mixtures were prepared in standard 1A gas cylinders. Refer to Appendix D for details. As shown, the system could accommodate as many as three gas cylinders. Since the helium, used for catalyst activation and free volume determinations, and the hydrogen, used for activation, were never disconnected, changing carrier composition required physically interchanging cylinders.

Upon expansion through a two stage pressure regulator, the gas passed first through a filter and then through a flow controller on its way to the precolumn, which was housed in the oven. The role of the precolumn was to remove any poisons which might be present in the feed stream. The sampling valve was located immediately downstream from the reference side of the thermal conductivity cell. An injected sample passed directly into the oven and hence the test column. Upon exiting the test column and the oven,

Numerical Legend

Figure III-1

1. Hydrogen
2. Helium
3. Carrier Gas
4. Pressure Regulator
5. Filter
6. Pressure Gage
7. Metering Valve
8. Flow Controller
9. Precolumn
10. Test Column Assembly
11. Sampling Valve
12. Thermal Conductivity Cell
13. Bridge
14. Ionization Chamber
15. Preamplifier
16. Electrometer
17. Recorder
18. Soap Bubble Meter
19. Oven

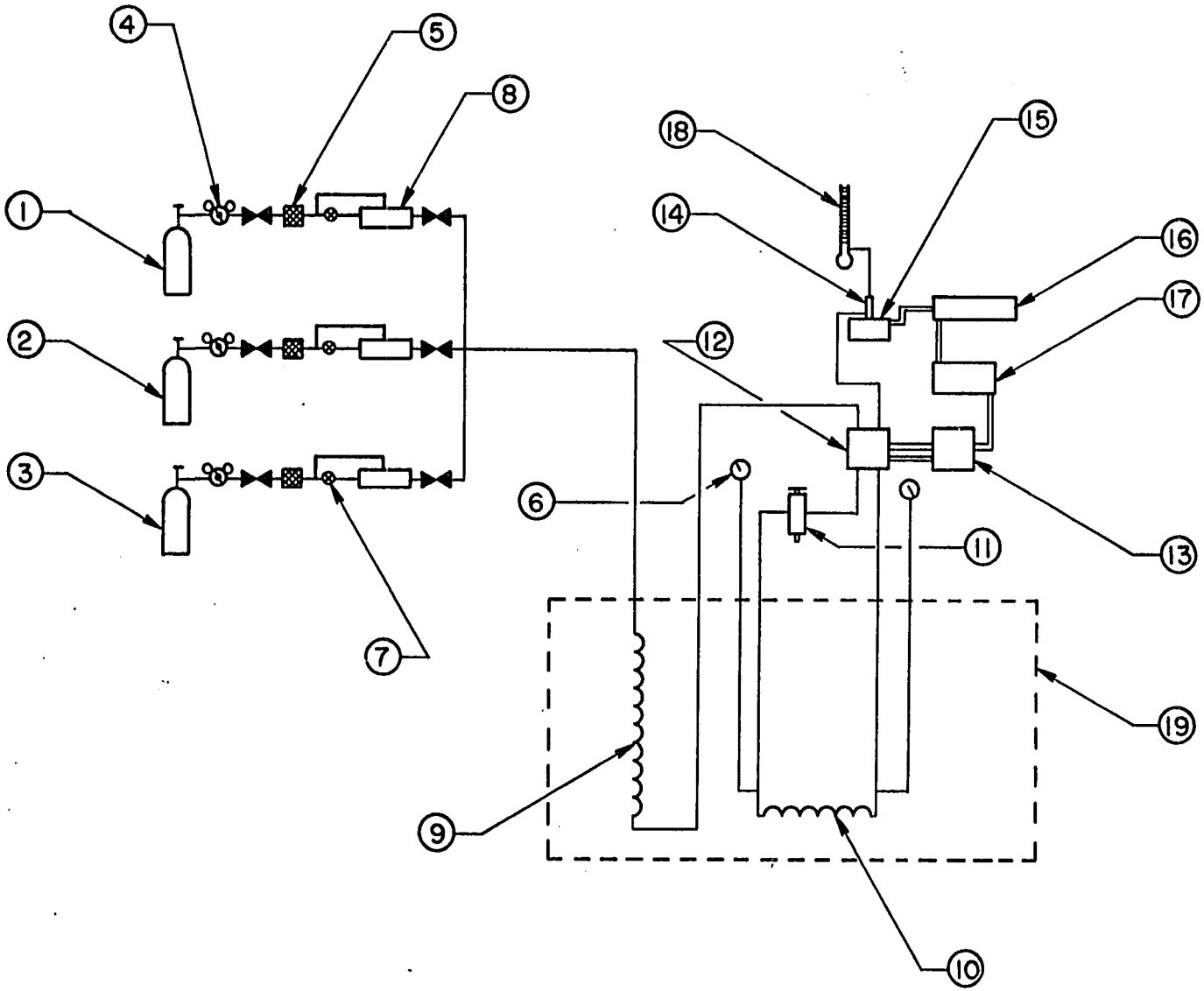

FIGURE III-1 SCHEMATIC FLOW DIAGRAM

the concentration peak was monitored in the sample side of the thermal conductivity cell. The effluent of the thermal conductivity cell entered the ionization chamber, where the radioactive tracer concentration was measured. The outputs of both detectors were recorded on a two channel chart recorder. The gas then exited through a 50 cc soap bubble flow meter to the hood, which exhausted to the atmosphere. Only the columns were thermostated; the remainder of the equipment was exposed to room conditions.

Two test columns were required in order to procure data over the desired range of residence times. Previous investigators (4, 38) used a capillary bypass, having a negligible residence time, to obtain a reference peak and thus eliminate the need to calibrate the system for lag time caused by dead volume and finite instrumentation responses. For experiments in which it was desired to maintain the residence time of the gas flowing through the column at a low value, the procedure resulted in unacceptably poor resolution of the two peaks. Therefore, the design shown in Figure III-2 was employed to overcome this problem. By interchanging line 1 and line 2 connections, flow could be directed either through the two columns in series or through the short column alone. In this manner the catalyst in both the short column and the long column had the same activation and temperature history. The bypass

Numerical Legend

Figure III-2

1. Short Column Entrance
2. Long Column Entrance
3. Plug
4. Oven
5. Short Column
6. Long Column
7. Pressure Gage
8. Toggle Valve
9. Bypass Line (for short column)
10. Bypass (for columns in series)

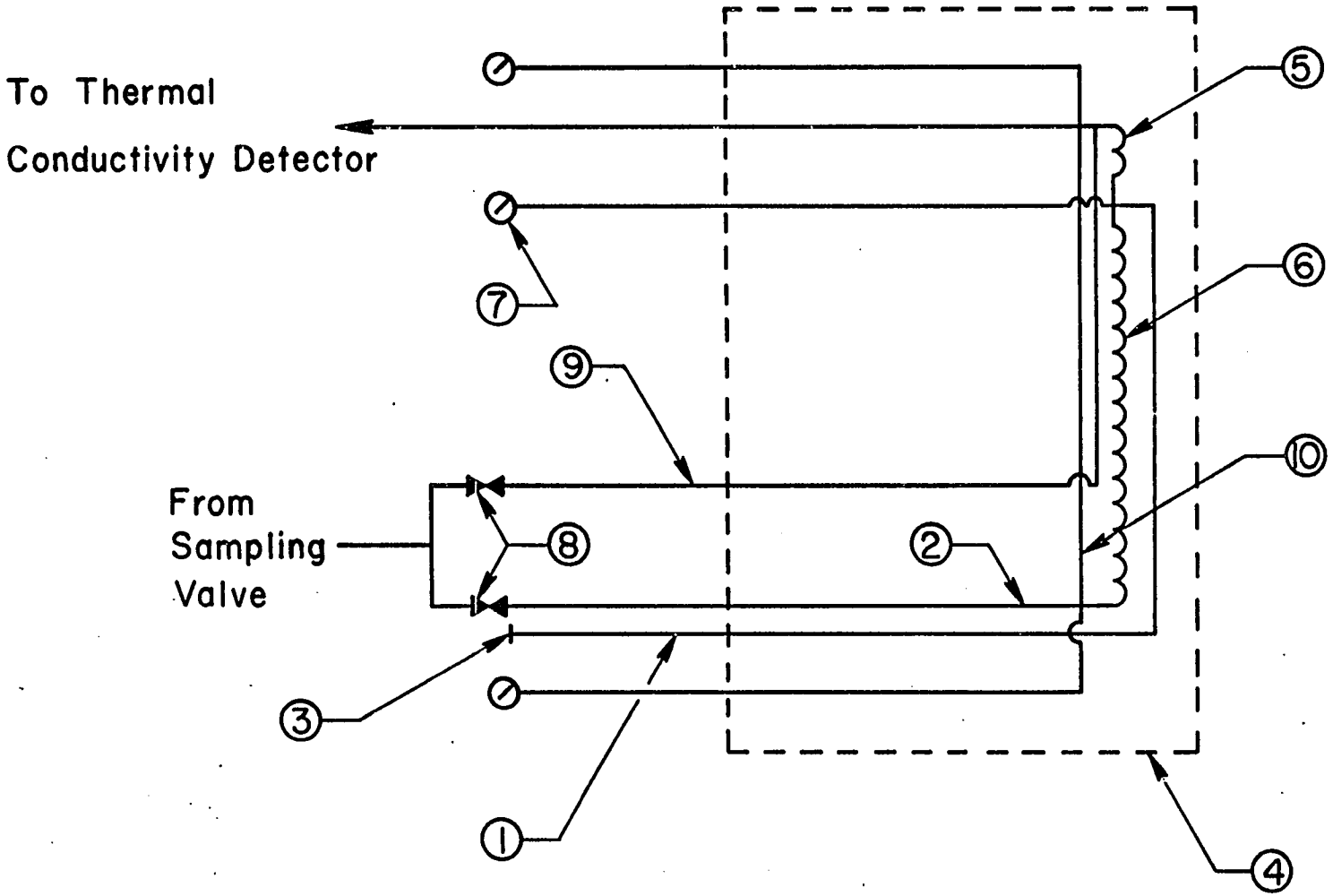

FIGURE III-2 TEST COLUMN ARRANGEMENT

could be used when the two columns were connected in series. When only the short column was in use, manipulation of the toggle valves directed flow either through the column or by the column. Therefore, the bypass and reference peaks could be obtained separately.

Pressure gages were used to measure column entrance and exit pressures, all of which were close to atmospheric. Mercury manometers were avoided because of the possible effects of the mercury vapor on the activity of the catalyst. The system could be evacuated on both sides of the precolumn and downstream of the test column.

A sample manifold, shown in Figure III-3, was constructed so that radioactive samples could be diluted and expanded into the sample loop for injection. An argon supply was connected to the manifold for free volume determinations. Details of the sample system can be found in Appendix C.

III.2 Procedure

Following activation, helium was passed over the catalyst in order to carry out bypass and free volume calibrations for both the long (series) and short columns. Upon completion of this procedure, a carbon monoxide-carbon dioxide carrier gas mixture of the desired concentration

Numerical Legend

Figure III-3

1. Stopcock
2. Breakseal
3. Ballbearing
4. $C^{14}O_2$ Supply
5. C^{14} O Supply
6. 30 cc Sample Container
7. Pressure Gage
8. Sampling Valve
9. Kovar Seal
10. Vacuum Pump
11. Sample Loop
12. External Inlet For Argon and Diluting Gases

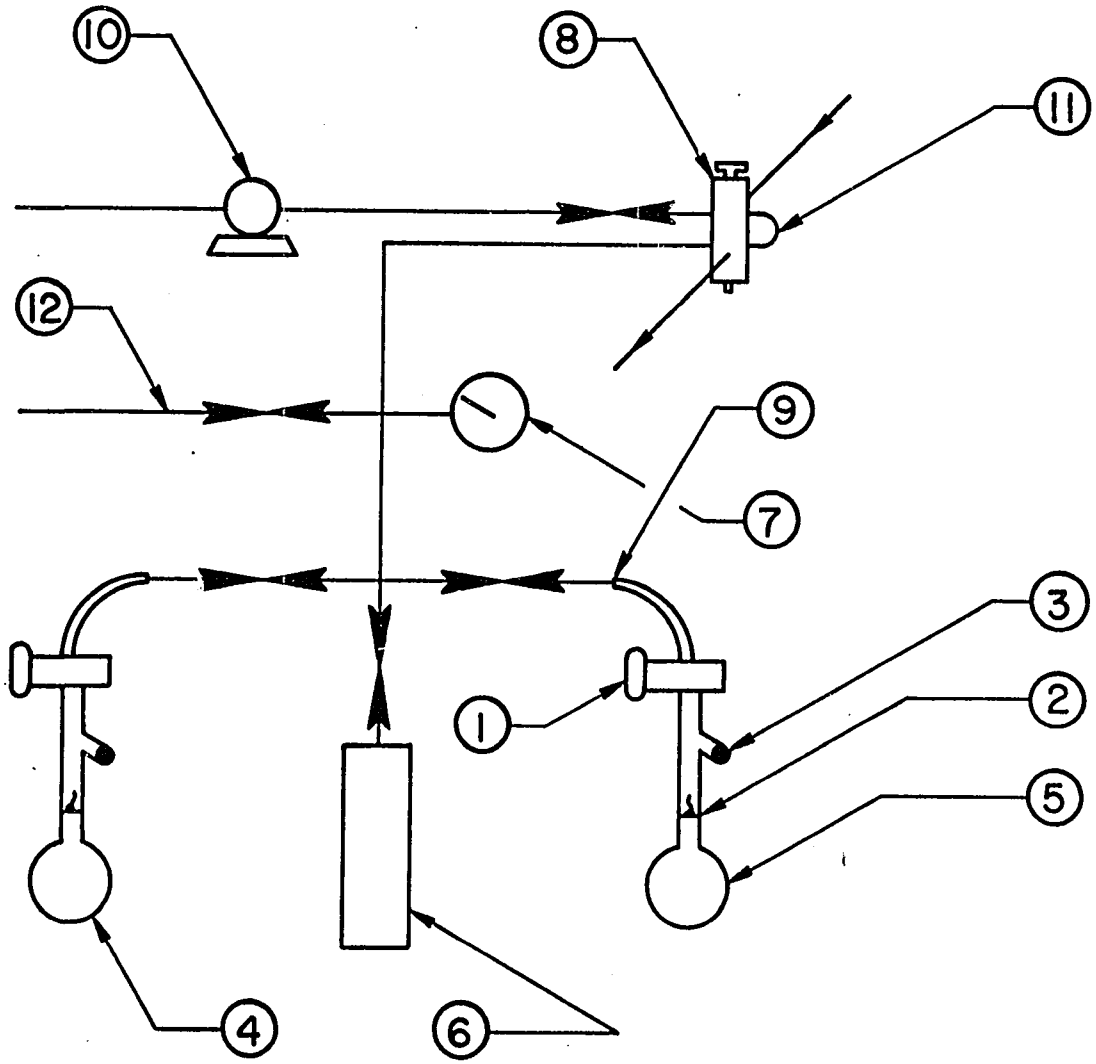

FIGURE III-3 SAMPLE SYSTEM

was allowed to flow slowly overnight over the catalyst in the long column. This procedure insured that any initial rapid catalyst deactivation was completed; and it allowed any helium, hydrogen, or water vapor trapped in dead ends, such as pressure gage connections, to diffuse outward. Experiments were then ready to be carried out in the long column.

The flow rate was established by opening the metering valve to the appropriate setting. When the thermal conductivity cell output indicated that the system had reached equilibrium, the flow rate was measured via the soap bubble meter. Simultaneously, oven temperature, inlet and outlet column pressures, room temperature, and barometric pressure were recorded. After the appropriate recorder range and chart speed were verified, carbon monoxide tracer was expanded into the sample manifold to a pressure of about 25" Hg vacuum. This pressure varied somewhat depending on the relative strength of the supply and the residence time of flow through the column. The sample then was injected via the sampling valve and the response was observed on the recorder. Since the long column (series configuration) was in use the output consisted of two peaks, the first due to the bypass and the second due to the column. The time elapsed between these peaks was treated as the residence time of the peak in the column. Determination of the peak

first moments is discussed in Appendix D.

After both tracers had been observed under these conditions, the metering valve was reset, and a new flow rate was established. The same data acquisition and sampling procedure was repeated.

For the high range of flow rates, the chromatographic train was reconnected so that experiments could be conducted over the short column. The experimental range of flow rates was limited by excessive pressure drop on the high end and by the minimum obtainable flow rate on the low end. The latter was determined by the flow controller capability and flow measurement accuracy.

For the short column, the procedure had to be modified slightly, however, because the bypass peak and the column peak had to be recorded separately as described earlier. The toggle valves first were positioned so that flow bypassed the column. After equilibrium conditions were attained, a sample of either tracer was expanded into the manifold. It was now necessary to mark the time of injection. This was accomplished by switching the chart movement switch to the off position and marking the pen position. Then, the chart movement switch was turned on simultaneously with injection of the sample. With the bypass peak thus recorded, the two toggle valve positions were reversed. When steady state was indicated, the same

set of data as described before was taken. Two samples were injected, one of each tracer, and the injection times were marked by the same procedure used for the bypass peak. As with the long column, flow rates were varied over a range with column and bypass samples being injected and data recorded at each point.

Upon completion of studies with a particular composition carrier gas, another mixture was investigated. The system was converted to the long column configuration and the new mixture was allowed to pass over the catalyst overnight. From this point the experimental procedure becomes identical with that already described for the first carrier gas.

Experiments with the helium-carbon dioxide carrier gas mixtures were abbreviated considerably with respect to the studies described previously. All data were taken at the same flow rate for the various mixtures. The work was conducted on the long column.

IV. RESULTS AND CONCLUSIONS

IV.1 Carbon Monoxide - Carbon Dioxide System

IV.1.1 Experimental Results

As was explained in Section III.2 the retention of both carbon monoxide and carbon dioxide tracers at 400°F and atmospheric pressure was recorded as a function of carrier gas residence time, t_r, for each carrier gas mixture. For each chromatogram the centroids of the bypass and main peaks were approximated by the procedure described in Appendix D. The difference between these two values was taken to be the residence time of the tracer in the column, t_p. This value was normalized to the flow rate by converting to the retention quantity G* according to equation (II-14).

$$G^* = \frac{1}{\beta} \left(\frac{t_p}{t_r} - 1 \right) \qquad \text{(II-14)}$$

The purpose of β is to give G* units of moles/g catalyst.

The experimental and calculated results for the carbon monoxide - carbon dioxide runs are tabulated in Appendices G and H, respectively. The results are plotted

in terms of G* versus $\ell n\ t_r$ in Figures IV-1 through IV-7. These data are the basis for this thesis.

The numbering of the carrier gas mixtures reflects the chronological order in which the experiments were conducted. Table C-1 lists the compositions of all carrier gases used in this work.

Originally it was hoped that by varying the residence time of the carrier gas (i.e., the velocity for a given column), it would be possible to define two distinct regions of behavior. This was based on the assumption that the surface exchange reaction step was a considerably slower process than either carbon monoxide or carbon dioxide adsorption on this catalyst. One region, corresponding to large values of t_r, would be characterized by the existence of adsorption and reaction processes all being at equilibrium. Within the limits of the other region, at low t_r values, the exchange reaction would be negligibly slow while the adsorption steps would remain essentially at equilibrium.

This approach met with little success, however, being too much of an oversimplification. As can be seen, the data generally are characterized by nonequilibrium processes; the existence of plateaus of constant G* is more the exception than the rule. Regions in which the equilibrium theory presented in Sections II.4.1 and II.4.3 is

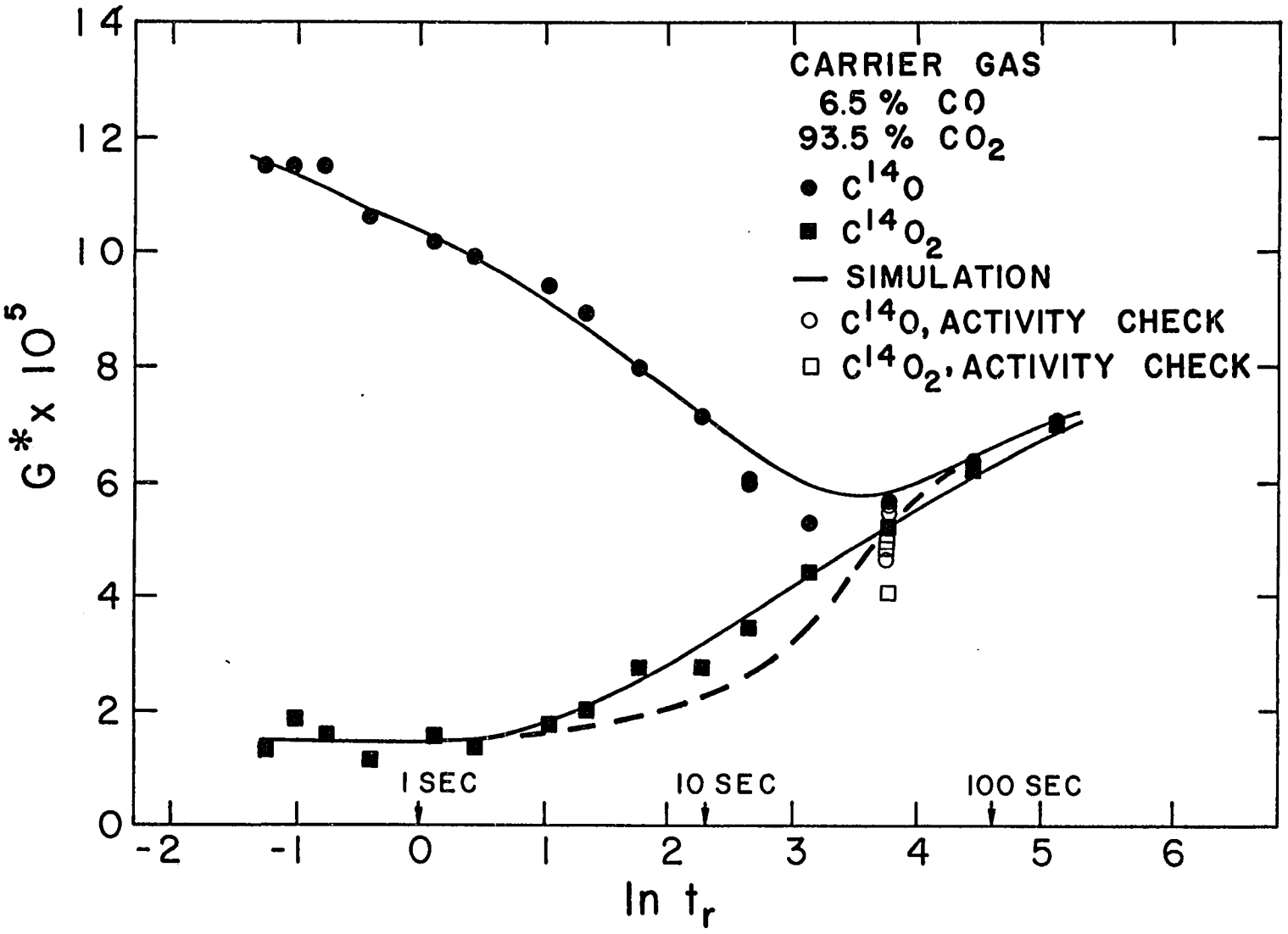

FIGURE IV - 1 G^* vs $\ln t_r$ - MIXTURE 1

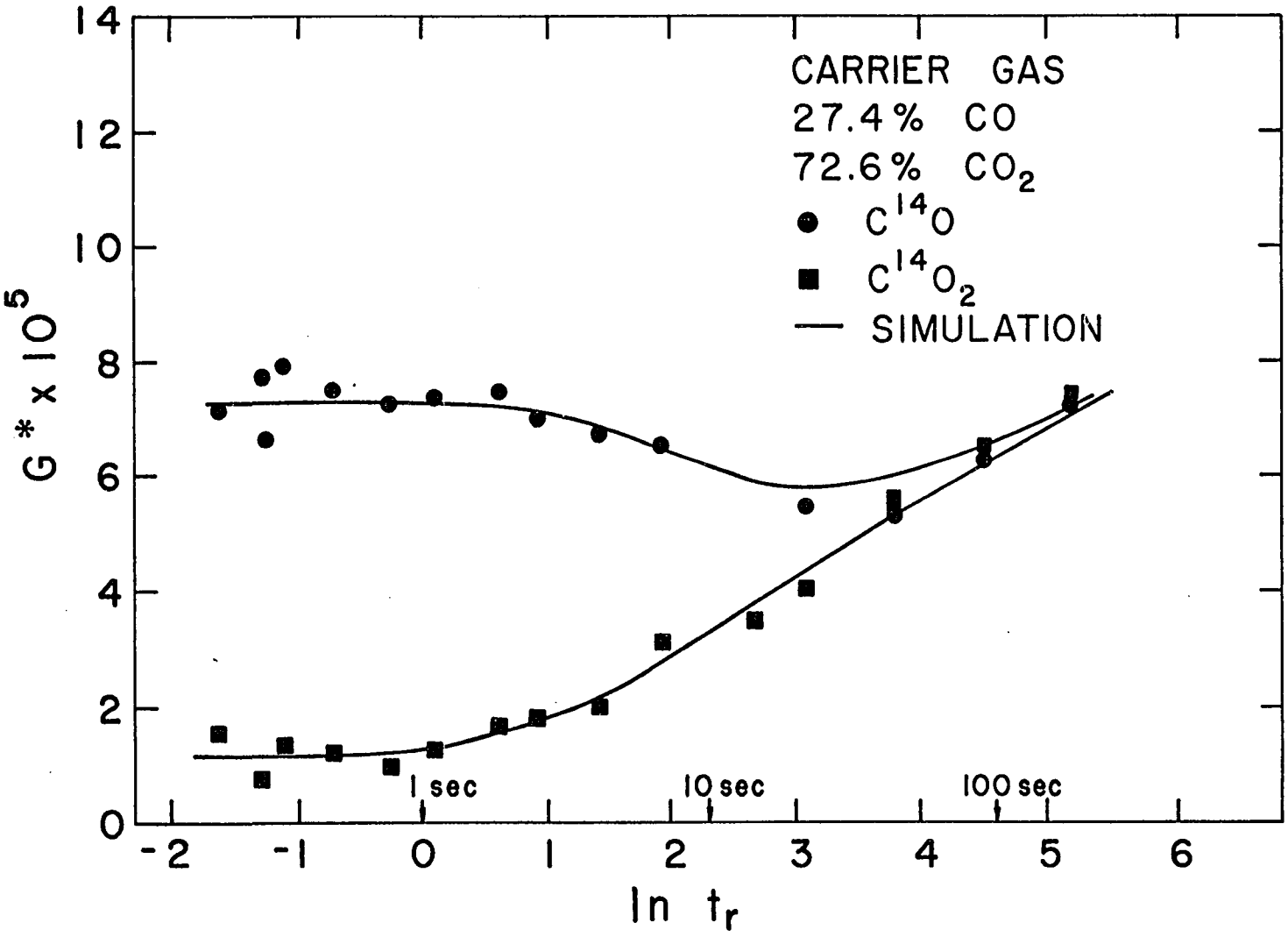

FIGURE IV - 2 G^* vs ln t_r - MIXTURE 2

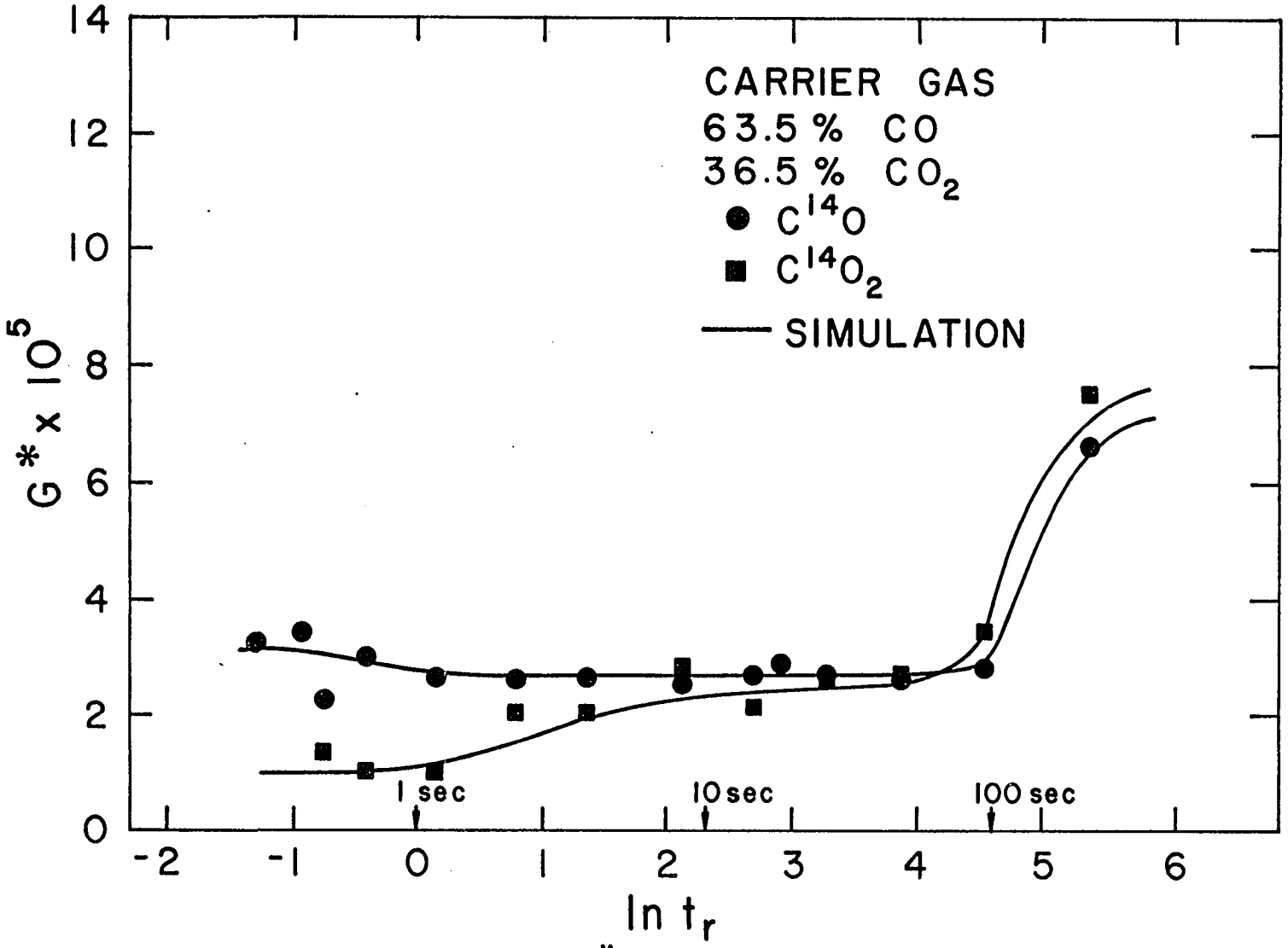

FIGURE IV - 3 G^* vs $\ln t_r$ - MIXTURE 3

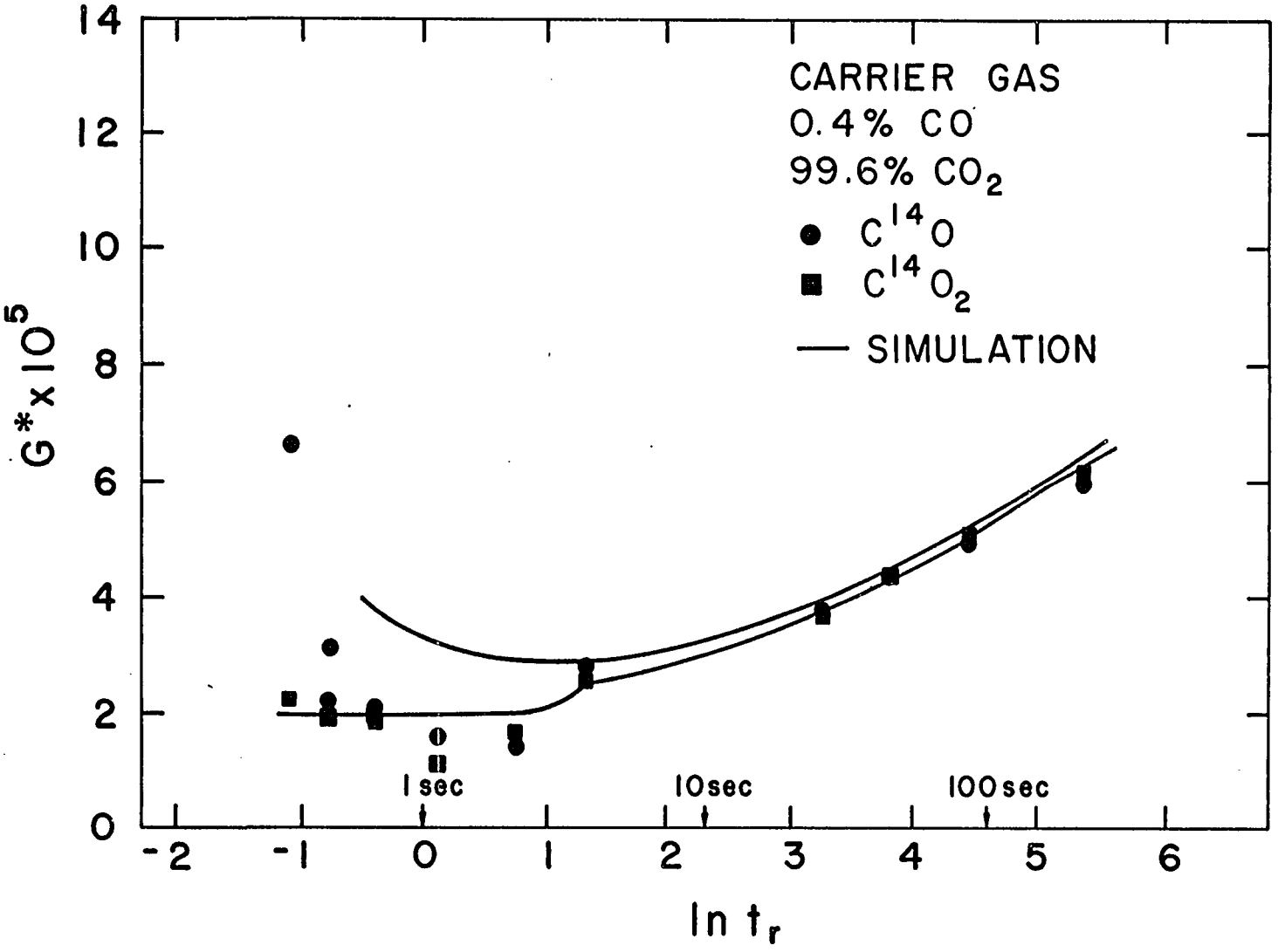

FIGURE IV-4 G^* vs $\ln t_r$ - MIXTURE 4

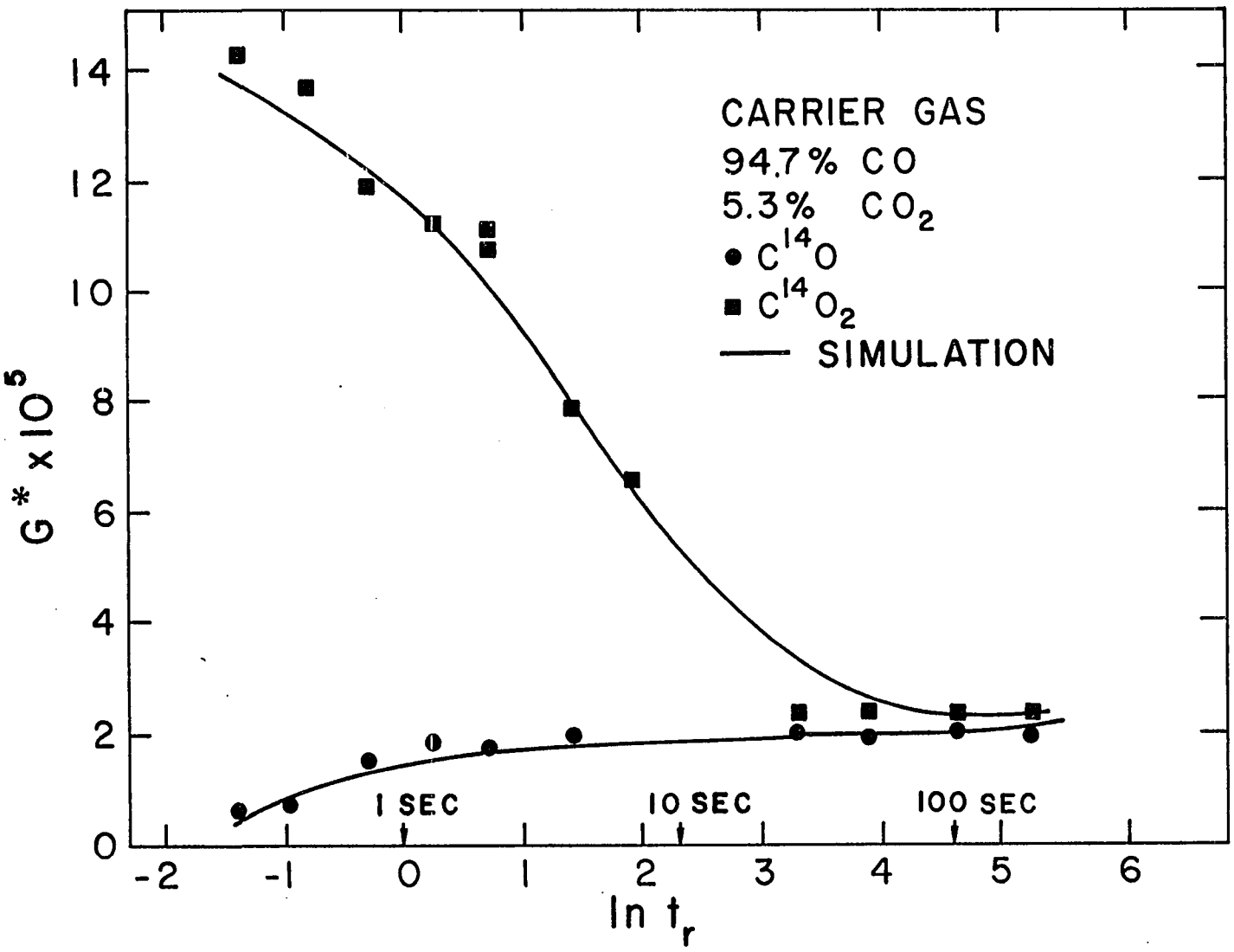

FIGURE IV-5 G^* vs $\ln t_r$ - MIXTURE 5

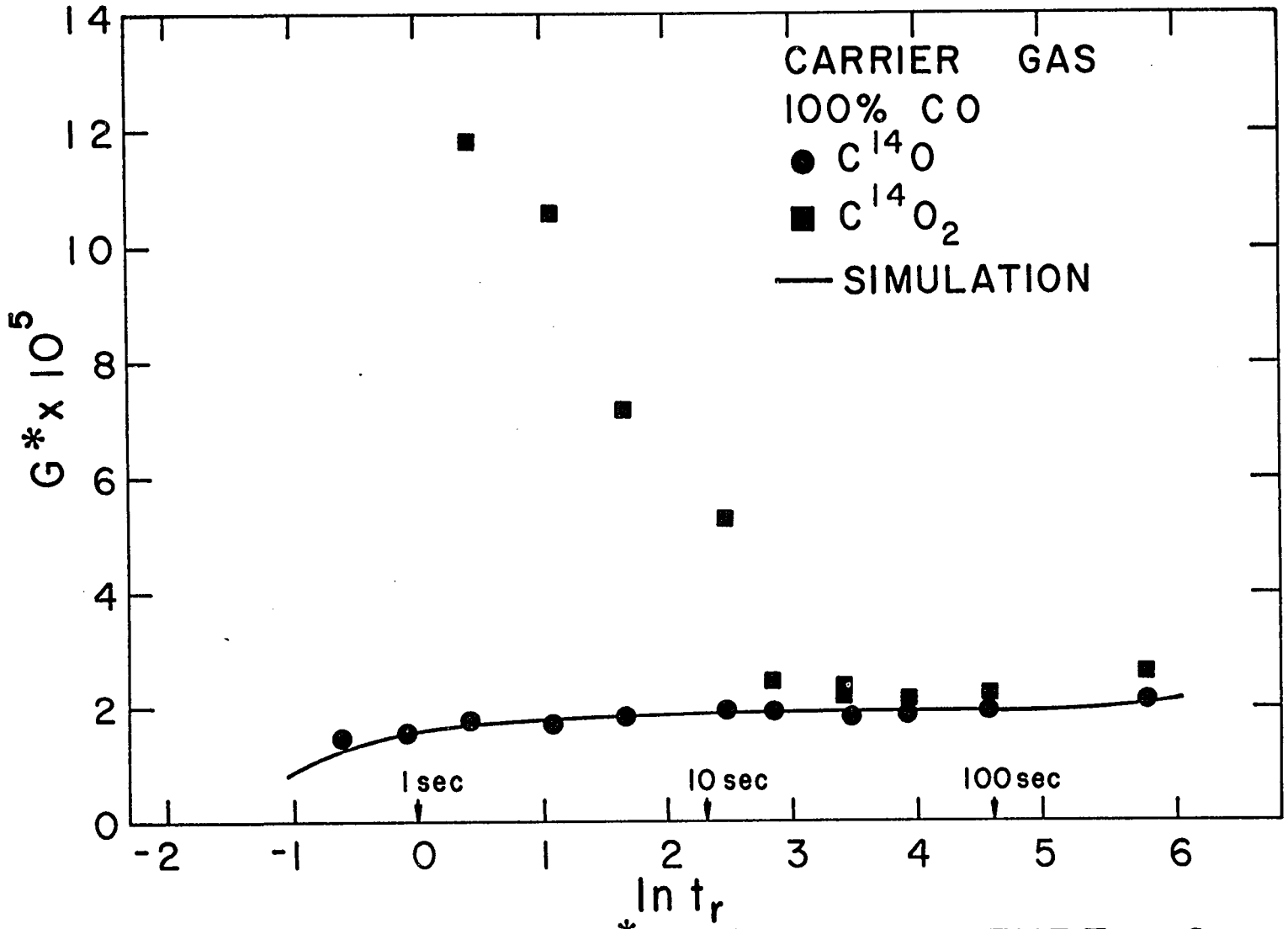

FIGURE IV-6 G^* vs $\ln t_r$ - MIXTURE 6

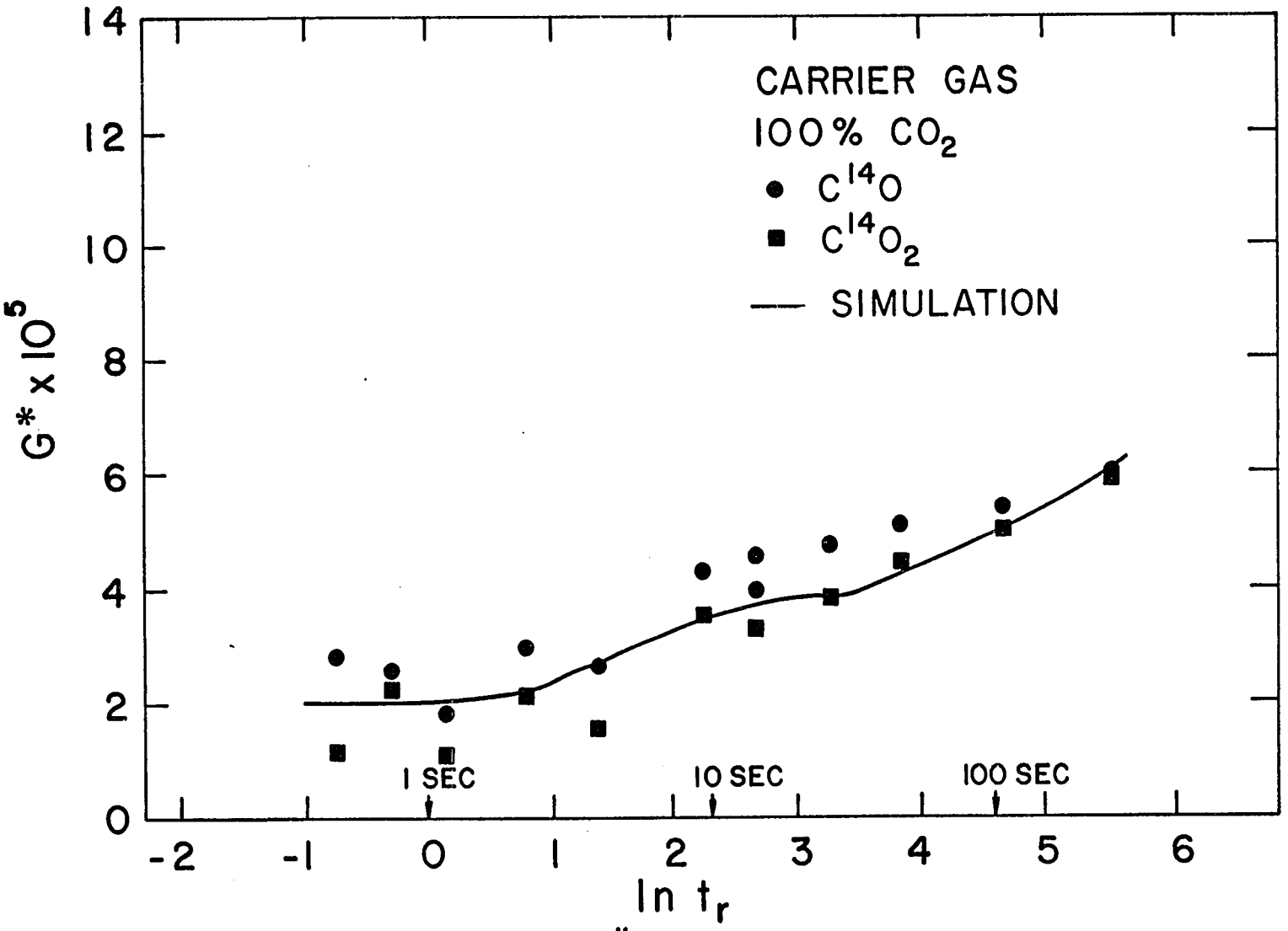

FIGURE IV - 7 G^* vs $\ln t_r$ - MIXTURE 7

valid will be pointed out in Section IV.1.3.

Qualitatively, several interesting features can be observed in Figures IV-1 through IV-7. In mixtures 1, 2, 4, and 7, which are rich in carbon dioxide, a slow adsorption process is evident because G* continues to increase even after the exchange reaction has apparently reached equilibrium. In mixtures 2 and 3 the retention of the carbon dioxide tracer at low t_r values is less than the carbon monoxide tracer; but as t_r becomes larger the carbon dioxide tracer eventually is retained longer than the carbon monoxide. This indicates that the slow adsorption process is a carbon dioxide step. Data taken with mixtures 3 and 5 also indicate that this slow carbon dioxide adsorption step is not necessary for the oxygen exchange reaction to proceed. It is also evident that as the carbon monoxide concentration in the carrier gas increases this carbon dioxide step becomes even slower until for mixture 5, it is beyond the range of experimental investigation. Contrasting the previously described type of adsorption is a fast form of carbon dioxide adsorption which is present at all seven carrier gas compositions.

Carbon monoxide, on the other hand, appears to adsorb rapidly in all cases except mixtures 5 and 6, in which at t_r values less than one second the G* value for the

carbon monoxide tracer appears to decrease.

IV.1.2 Column Simulation

As was pointed out in Section IV.1.1, the data generally were characterized by nonequilibrium processes, which invalidated the assumptions leading to the solutions to the equations presented in Sections II.4.1 and II.4.3. It was necessary to solve the rate equations numerically in order to describe the data over the entire range of t_r.

The column was simulated by a number of perfectly mixed tanks in series according to the method of Deans and Lapidus (10). A copy of the Fortran program is included in Appendix I. In this system the column dispersion amounted to only a small fraction of the dispersion created by the kinetic processes involved. As a result it was possible to reduce the number of tanks used to approximate the column to thirty without affecting the results. This was checked several times by using 45 and 60 tanks. The output in each case was unchanged. The retention time of the simulated peak was determined by the same method used for the experimental peaks; that is, the centroid of each peak was approximated by the procedure described in Appendix D instead of using the peak maximum as a time reference.

Several mechanisms advanced to describe the adsorption processes in this system were found to be unsatisfactory.

The five step scheme presented in Section II.4.2 proved to explain the data where the others failed. This is not to say that this mechanism is a unique description of the system. It does, however, combine simplicity with qualitative agreement. Three adsorption steps and a reaction step were pointed out in Section IV.1.1. The fifth step had to be added in order to simulate the data satisfactorily.

It was originally hoped that the constants K_ℓ and k_ℓ, in equations (II-36) and (II-43), respectively, would fit the data over the entire range of carrier gas compositions. After three sets of data (carrier gas mixtures) had been roughly fit, it became obvious that K_ℓ and k_ℓ were not constant over the entire range of carrier gas compositions. Therefore, the data for each mixture were fit according to the following modified version of the mechanism presented in Section II.4.2.

1. $CO \rightleftarrows (CO)_A$
2. $CO \rightleftarrows (CO)_B$
3. $CO_2 \rightleftarrows (CO_2)_B$
4. $X + (CO_2)_B \rightleftarrows (CO)_B + XO$
5. $CO_2 \rightleftarrows (CO_2)_C$

where: X = any oxygen acceptor

$(i)_M$ = component "i" on site "M"

The equilibrium functions in the above kinetic scheme remain identical to those listed in equations (II-38). The rate parameters, k'_ℓ, for the above steps become, in terms of those in equations (II-43)

$$k'_1 = k_1 A \qquad \text{(IV-1a)}$$

$$k'_2 = k_2 B \qquad \text{(IV-1b)}$$

$$k'_3 = k_3 B \qquad \text{(IV-1c)}$$

$$k'_4 = k_4 \qquad \text{(IV-1d)}$$

$$k'_5 = k_5 C \qquad \text{(IV-1e)}$$

There are some subtle differences between this scheme and the mechanism presented in Section II.4.2 which merit discussion. In step 4, which provides the coupling between the two tracers, it now becomes impossible to distinguish between a direct oxygen transfer process and the dissociation of molecularly adsorbed carbon dioxide. It is also no longer possible to differentiate between sites "A" and "C". That is, the carbon monoxide and carbon dioxide adsorption processes, steps 1 and 5, which are not involved directly in the surface exchange reaction may or may not occur on the same sites.

Perhaps the most interesting difference between the two mechanisms is that the former assumes Langmuir behavior and the latter does not. One of the assumptions on which the Langmuir adsorption model is based is that the surface is energetically uniform. This is often quite unrealistic, and the results of Section IV.2.2 demonstrate this with respect to carbon dioxide adsorption on this catalyst.

As stated earlier, no one set of constants could be found which fit all the data. For this reason no attempt was made to use statistical methods to minimize the error between the simulated results and the experimental data. The fact that quantitative agreement can be achieved is apparent from Figures IV-1 through IV-7. It should be pointed out that for carbon dioxide tracer in pure carbon monoxide carrier gas, numerical simulation was not possible because the equilibrium function for the surface reaction step becomes infinite. Simulation was also not possible in the opposite case, carbon monoxide tracer in carbon dioxide carrier gas, because the surface reaction equilibrium function equals zero. Consequently, the last term in equation (II-43d) becomes infinite.

The results of the numerical studies indicated that some of the adsorption processes were, in fact, more rapid than others. Table IV-1 gives a qualitative classification

of five kinetic steps according to relative speed.

TABLE IV-1 Relative Rates of the Various Steps

Step 1	Carbon monoxide adsorption	fast
Step 2	Carbon monoxide adsorption	slow
Step 3	Carbon dioxide adsorption	fast
Step 4	Surface reaction	moderate
Step 5	Carbon dioxide adsorption	slow

Equilibrium and rate parameters in equations (II-38) and (IV-1) used to account for the results in Figures IV-1 through IV-7 are shown in Table IV-2. The equilibrium constant K_4' is omitted because, as is shown in Appendix A, it is not an independent variable. Once again it should be emphasized that these numbers are of a qualitative significance only. In some cases the results were insensitive to certain of the parameters. The numbers used in these cases are not to be taken seriously.

Contradicting the hypothesis advanced in Section IV.1.1, the results of this study show that the surface reaction is not the slowest step. One of the types of both carbon monoxide and carbon dioxide adsorption is apparently slower than step 4. An interesting consequence is that

TABLE IV-2 Equilibrium and Rate Parameters[†]

Mixture	7	4	1	2	3	5	6
μ_{CO}^{A}	6.0	6.0	4.87	3.34	1.3	0.73	0.87
μ_{CO}^{B}	208.*	208.*	13.0	3.34	0.22	0.34	0.36
$\mu_{CO_2}^{B}$	0.84	0.84	0.67	0.57	0.47	0.1*	u
$\mu_{CO_2}^{C}$	1.34	1.34	1.44	1.38	6.96	u	u
$\frac{Q\ k_1'}{V_t}(sec)^{-1}$	e	e	e	e	e	4.0	5.3
$\frac{Q\ k_2'}{V_t}(sec)^{-1}$	e	e	0.22	.096	0.21	.011	.013
$\frac{Q\ k_3'}{V_t}(sec)^{-1}$	e	e	e	e	e	e	e
$\frac{Q\ k_4'}{V_t}(sec)^{-1}$	0.43	0.43	0.60	0.55	0.90	e	u
$\frac{Q\ k_5'}{V_t}(sec)^{-1}$	.017	.017	.021	.016	.063	u	u

[†]The equilibrium parameters in Table IV-2 can be converted to the form of equation (II-15) by dividing by β. Although, strictly speaking, β varies with the flow rate, i.e., with the pressure drop, an approximate value for β is 0.43×10^5 g/g mole.

*Denotes that the simulation was insensitive to this parameter.

[e]Denotes that the rate parameter was set sufficiently high to insure equilibrium at all times.

[u]Denotes that this step was unnecessary to explain the data, so the rate constant was set at zero.

carbon monoxide adsorption, step 2, is the rate limiting step for the exchange reaction. This is surprising in that one might intuitively expect carbon dioxide adsorption, especially if it were dissociative in nature, to be slower than the carbon monoxide adsorption.

For example, Cha and Parravano (7) concluded that the rate limiting step in the titanium dioxide catalyzed oxygen exchange reaction was the carbon dioxide adsorption step. Furthermore, their calculations indicated that the subsequent dissociative breakdown of the adsorbed carbon dioxide was much faster than the molecular adsorption step.

That more than one type of adsorption for both carbon oxides is required to explain the data is not surprising. In Section I.2 it was stated that infrared studies (1, 51) indicated more than one type of carbon monoxide adsorption on zinc oxide. The added presence of more than one form of copper (54) on the surface of this catalyst leads to the conclusion that the surface is quite heterogeneous.

As was previously stated, this study was unable to determine whether the surface reaction proceeded via direct oxygen transfer or dissociative carbon dioxide adsorption. It can, however, be emphasized that the literature favors the copper as the active portion of the catalyst with respect to the exchange reaction. Two sources, Winter (56)

and Nekipelov and Kasatkina (39), stated that the exchange reaction was negligible over zinc oxide. In the latter paper it was further argued that dissociative carbon dioxide adsorption did not occur on zinc oxide. Stroeva et al. (48), however, did observe this reaction to be catalyzed by copper. Their results also indicated that the copper existed primarily in the metallic state. The nature of carbon dioxide adsorption on copper at this temperature is still open to question, however. Hayward and Gomer (23), for instance, found both associative and dissociative carbon dioxide adsorption on tungsten, and the same situation may well exist for copper.

A salient feature which was not noticed until the simulation studies were carried out is that for mixtures 1, 2, 4, and 7, the carbon dioxide G* values increase linearly with respect to $\ell n\ t_r$ at sufficiently large values of t_r. This property could not be explained by one rate process alone because of the large range of t_r involved. Attempts to do this resulted in a serpentine approximation of the straight line. An attempt to describe this feature by two successive rate processes, steps 2 and 5, was still unsuccessful, as evidenced by the dashed curve in Figure IV-1. However, a series of three rate processes, or transformations during which additional steps become appreciable,

gives a much better approximation of this apparently linear relationship.

Figure IV-1 is a good example of this finding. At very low t_r values, G* for the carbon dioxide tracer is due to step 3 alone, with the subsequent surface reaction step and the slow carbon dioxide adsorption step both too slow to contribute to the observed response. As t_r increases the surface reaction of the adsorbed carbon dioxide begins to become important. This increases the amount of adsorption, and consequently G* begins to increase. The exchange reaction is not yet at equilibrium, however, because the carbon monoxide adsorption in step 2 is still negligibly slow. Just as this change in G* has passed the inflection point and has begun to start leveling out, another process becomes important. This process is the approach to the equilibrium reaction provided by steps 2, 3, and 4. Using the equilibrium values for steps 1 through 4, equation (II-42) predicts the new value of G*, which in this case is larger than that provided by carbon dioxide adsorption alone. Finally, after this process has nearly reached equilibrium, a third process begins to become important. Step 5, the slow carbon dioxide adsorption step, contributes to the last stage of the increase in G*. Presumably, if there are no unaccounted for adsorption steps, G* would finally level off at a value predicted by equation (II-35).

The greatest difficulties in fitting the data arose in mixtures 4 and 7, which are both almost pure carbon dioxide. In both cases carbon monoxide tracer was rapidly converted to carbon dioxide. Numerically it was not possible to obtain this degree of conversion without jeopardizing the carbon dioxide fit. This may suggest that under these conditions, in which the surface may contain a significant amount of oxygen, a competing step leading to the exchange reaction exists. Although there is no direct supporting evidence, a possible parallel mechanism might be

$$CO + \overset{O}{\overset{|}{S}} \rightleftarrows CO_2 + S$$

Another source of error is the extreme sensitivity of the numerical simulation to carrier gas composition when the mole fraction of one of the components nears zero. The analysis of mixture 4 was not very accurate because of the minimal amount of carbon monoxide present. Also, mixture 7 was classified as being 100% carbon dioxide, although the impurities may be as high as 0.5% as stated in Appendix B. Since one of the major impurities is carbon monoxide, the minimal differences between the data in Figures IV-4 and IV-7 are not surprising. It should also be added that explanation of the carbon dioxide data in Figure IV-7

required the presence of a small amount of carbon monoxide. Otherwise the linear variation of the carbon dioxide data discussed previously could not be simulated.

IV.1.3 Equilibrium Regions

After the numerical simulations were carried out, it became easier to locate the plateaus in G* where the analytical solutions of the theory presented in Sections II.4.1 and II.4.3 were valid. The following is a summary of regions in the various figures where these solutions hold:

Figure IV-1: At very low t_r values, G* for the carbon dioxide data is approximately constant. This can be explained by assuming that step 3 is near equilibrium while the surface reaction step (step 4) is negligible. This situation is expressed by equation (II-41).

$$G^* = \mu_{CO_2}^{B'} \qquad \text{(II-41)}$$

Figure IV-2: These results are similar to those in Figure IV-1. In addition, at low t_r values carbon monoxide adsorption is due only to step 1 and can be described by equation (II-40).

$$G^* = \mu_{CO}^{A'} \qquad \text{(II-40)}$$

Figure IV-3: The low t_r behavior of both carbon monoxide and carbon dioxide can be explained as in Figure IV-2. In this case, however, a new plateau becomes evident in which the reaction is at equilibrium and the slow carbon dioxide adsorption step is still negligible. The region is defined roughly by $10 < t_r < 50$ seconds. The value of G* is predicted by equation (II-42). Using the values for the equilibrium constants that were found while fitting the data, the predicted value of G* is 2.69×10^{-5}, which is to be compared with the experimental value of approximately 2.7×10^{-5}.

$$G^* = y^s_{CO}\ \mu'_{CO} + y^s_{CO_2}\ \mu^{B'}_{CO_2} \qquad \text{(II-42)}$$

Figure IV-4: This case is the same as Figure IV-1.

Figure IV-5: Carbon monoxide adsorption in a t_r range of $1 < t_r < 100$ seconds can be described by equation (II-40).

Figure IV-6: This case is the same as Figure IV-5.

Figure IV-7: This case is the same as Figure IV-1.

IV.2 Carbon Dioxide - Helium System

IV.2.1 Basis for Experiments

The oxygen exchange reaction can conceivably occur

through either an associative carbon dioxide adsorption step with subsequent oxygen transfer to an adjacent carbon monoxide species, or a dissociative mechanism, in which surface oxygen and carbon monoxide species are formed. This latter step is represented by steps 3 and 4 in Section II.4.2. In the past chromatography has been used to distinguish between various types of adsorption. The theory presented in Appendix A can be applied to carbon dioxide if it is assumed that any carbon monoxide formed on the surface does not desorb as such. This assumption was verified in Section IV.1.2, in which simulation studies indicated that the desorption of carbon monoxide was indeed very slow. It is therefore desirable to distinguish between the two following carbon dioxide adsorption mechanisms:

$$CO_2 + S \rightleftarrows \overset{CO_2}{\underset{|}{S}} \qquad \text{(associative)}$$

$$CO_2 + 2S \rightleftarrows \overset{O}{\underset{|}{S}} + \overset{CO}{\underset{|}{S}} \qquad \text{(dissociative)}$$

Indication that dissociative carbon dioxide adsorption might occur on this catalyst was obtained from the experiment discussed in Section IV.1. In Figure IV-8 plots of $\ell n\ G^*$ as a function of t_r are shown for the two carrier gases with the minimum carbon dioxide to carbon monoxide

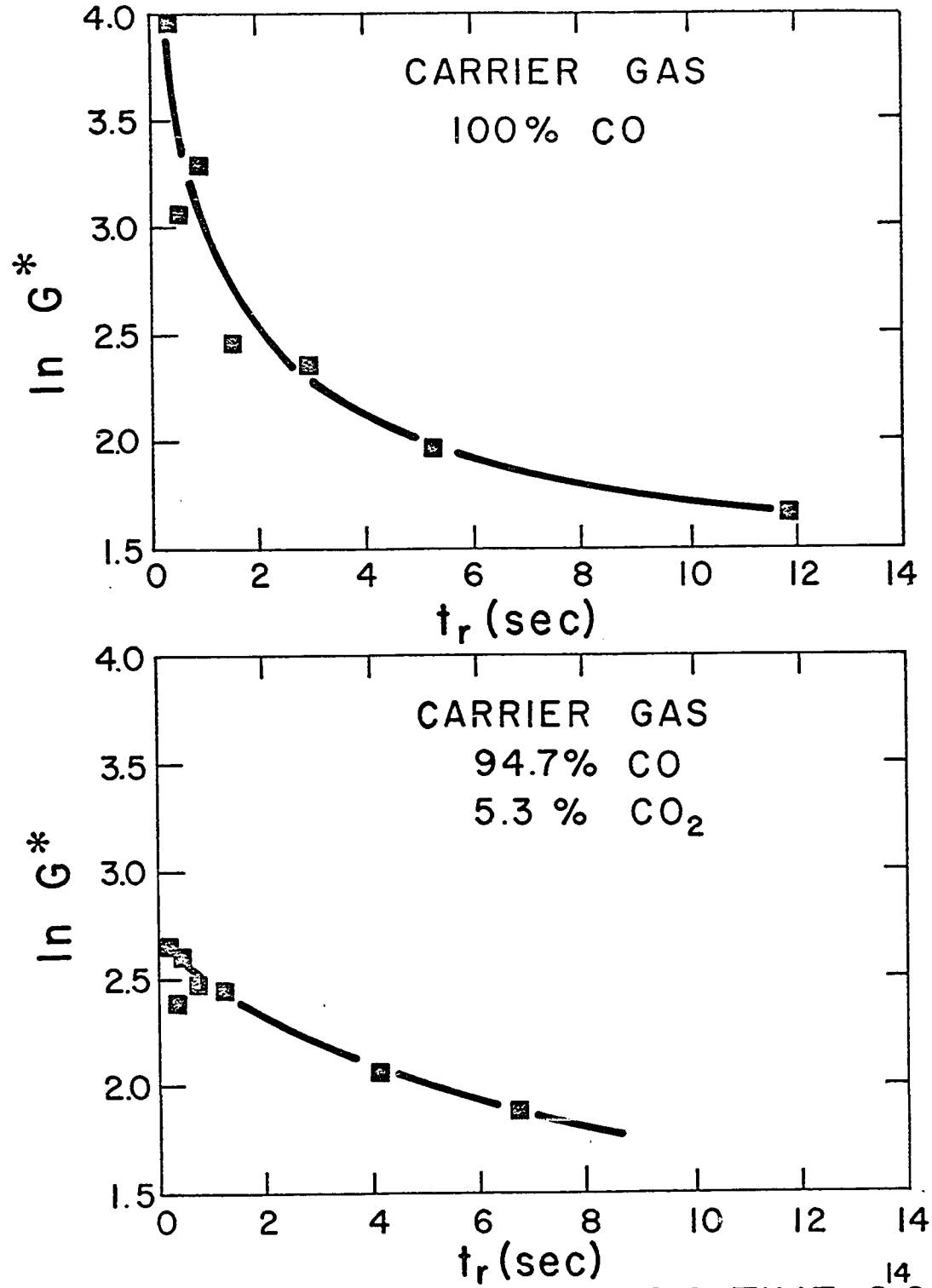

FIGURE IV-8 LOW RESIDENCE TIME $C^{14}O_2$ DATA IN RICH CO CARRIER GASES

ratio. These results show that as y_{CO_2} becomes small, the limiting value of G*, as t_r approaches zero, becomes very large. Furthermore, G* at low t_r values is due primarily to adsorption and not reaction. According to equation (A-6), this type of behavior is to be expected when dissociative Langmuir adsorption is present. Data for carbon monoxide samples in rich carbon dioxide carrier gases, shown in Figure IV-9, can be seen to contrast this type of behavior. In this case the limiting values of ℓn G* do not seem to increase in the same manner as the data in Figure IV-8.

IV.2.2 Experimental Results

It was decided therefore to conduct a brief investigation of the carbon dioxide - helium system. The raw data and calculated results for the six carrier gases used are shown in Appendices G and H, respectively. The same flow rate was used in all cases, and, as with the carbon monoxide-carbon dioxide system, all work was carried out at 400°F and atmospheric pressure. The experiments were abbreviated for two reasons. First, since the simulation work had not yet been completed by the time these experiments were conducted, it was not known whether or not the dissociative theory could be applied. Second, the absence of carbon monoxide in the carrier gas might tend to leave most of the

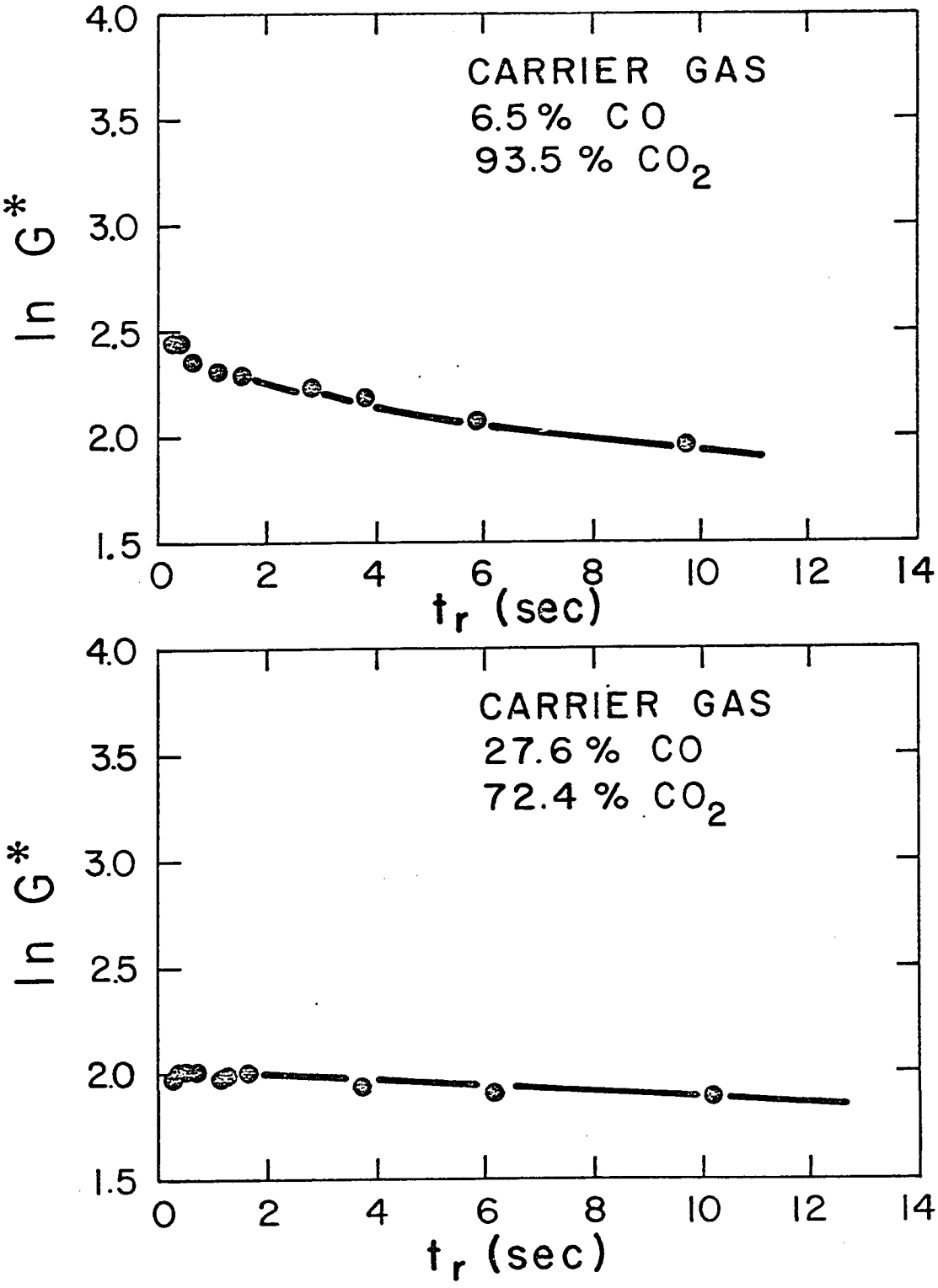

FIGURE IV-9 LOW RESIDENCE TIME $C^{14}O$ DATA IN RICH CO_2 CARRIER GASES

sites oxygenated if dissociative adsorption did occur. The resulting surface, then, might be very much unlike the one over which the experiments with the carbon monoxide - carbon dioxide system were completed.

The results shown in Appendix H show that G* increases as y_{CO_2} approaches zero. If Langmuir two site adsorption exists equation (A-7) should be valid, and the product G* $y_{CO_2}^{1/2}$ should approach a constant as y_{CO_2} approaches zero. In Figure IV-10 the data are plotted in this form. It is quite apparent that this relationship does not hold.

At this point it was decided to check for Freundlich behavior. The form of G* for a Freundlich isotherm is presented in Appendix A. A plot of ℓn G* versus ℓn y_{CO_2}, which is indicated by equation (A-10), is shown in Figure IV-11. The resulting straight line demonstrates that a Freundlich isotherm does explain the data. The value of the constant d in this case is -0.84. The Freundlich isotherm can be derived by assuming that the heat of adsorption varies exponentially with surface coverage. Consequently, the assumption of a constant heat of adsorption, as required by the Langmuir model, has been demonstrated to be invalid.

IV.3 Conclusions

Chromatography and, more specifically, the use of

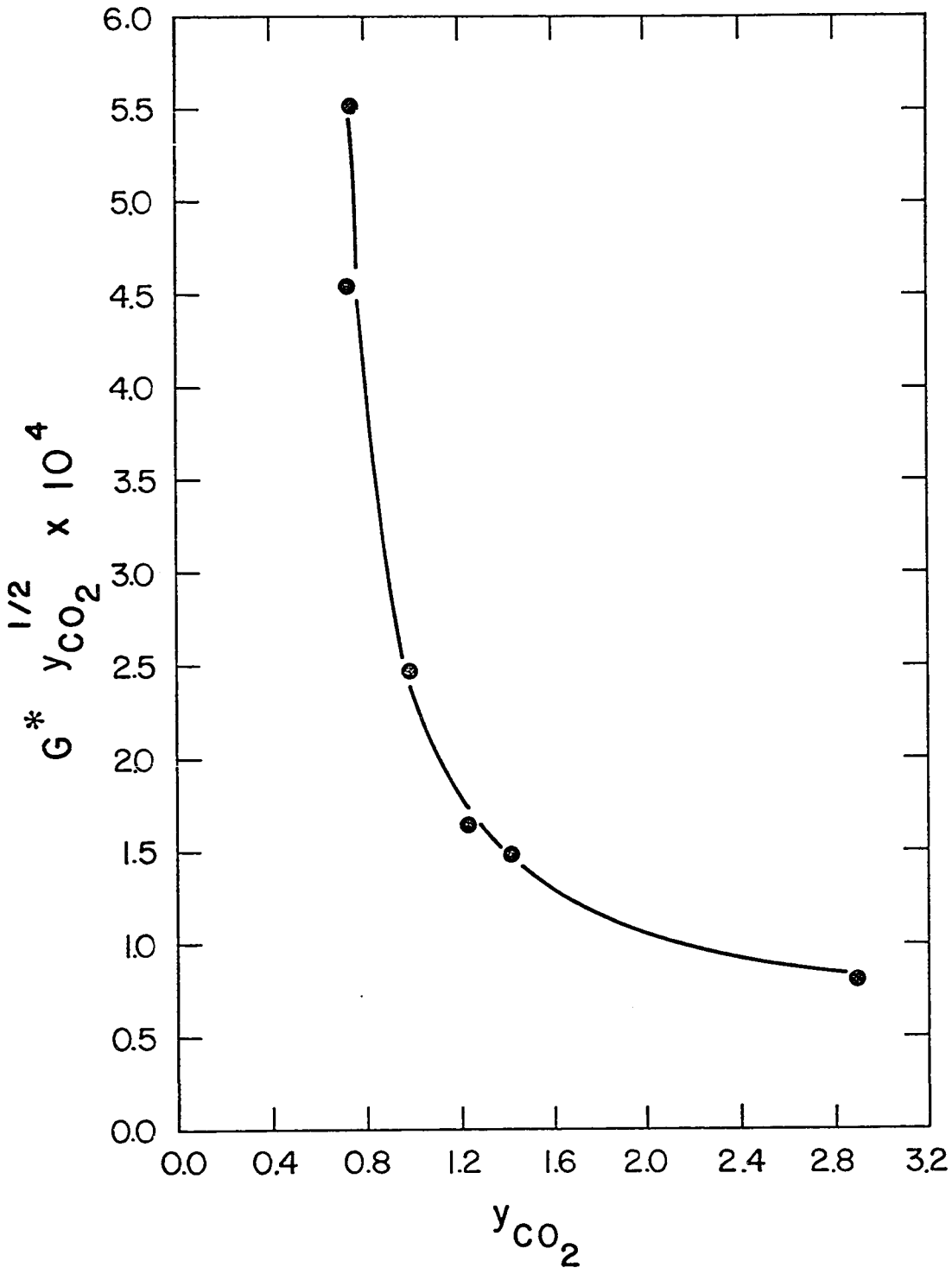

FIGURE IV-10 LANGMUIR TWO SITE ADSORPTION TEST FOR CO_2

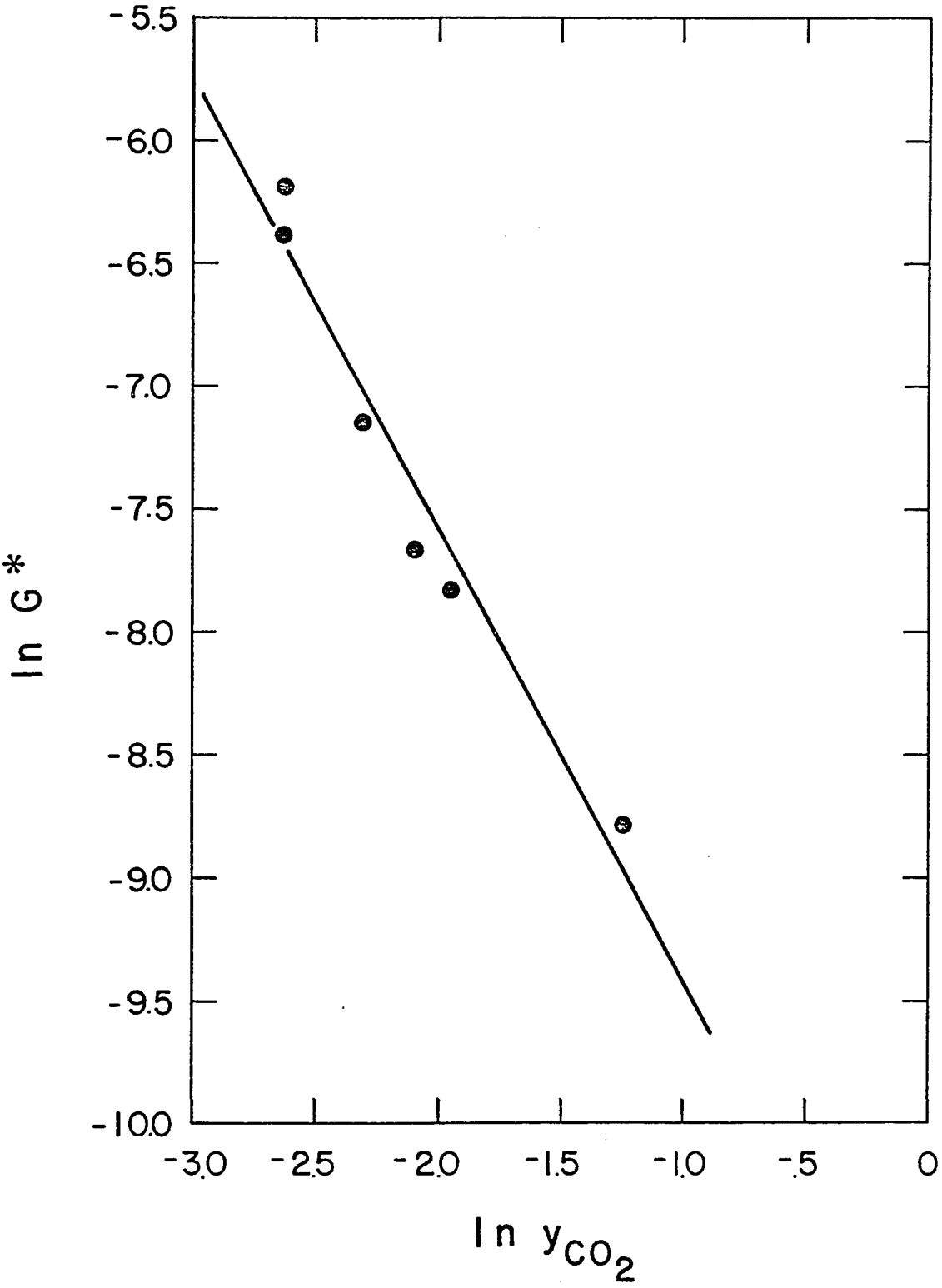

FIGURE IV-11 FREUNDLICH TEST FOR CO_2 - HE SYSTEM

isotopic tracers have once again been demonstrated to be an effective tool for investigating adsorption phenomena. In this case, the extension to cases involving nonequilibrium reactions has resulted in a somewhat more difficult theoretical problem. Several conclusions have been reached, however, by this method regarding the carbon monoxide - carbon dioxide system in the presence of a copper - zinc oxide catalyst at 400°F.

1. Based on the mechanism used to explain the data, there are at least two types of carbon monoxide adsorption on this catalyst. One form is rather rapid while the other is considerably slower. The slower form is involved in the oxygen exchange reaction.

2. Similarly there are two types of carbon dioxide adsorption, but in this case the faster process leads to the exchange reaction.

3. The rate limiting step in the exchange reaction has been found to be a carbon monoxide adsorption step.

4. The surface of this catalyst has been found to be energetically heterogeneous. This is indicated by the inability to fit a Langmuir model to the data and by the Freundlich nature of the carbon dioxide adsorption.

5. Attempts to distinguish between associative and dissociative carbon dioxide adsorption have been inconclusive.

6. The effect of varying the carrier gas flow rate has been demonstrated an important one. This result casts some doubt on the reliability of chromatographically determined isotherms on surfaces where nonequilibrium processes may be present despite being assumed nonexistant.

APPENDIX A

THEORETICAL DETAILS

A.1 Associative Adsorption

Consider a gas which only adsorbs molecularly on the surface of the catalyst. The Langmuir equilibrium relation takes the following form:

$$n_i' = \frac{a\, y_i}{1 + b\, y_i} \qquad \text{(A-1)}$$

where: a, b are constants at a given temperature

When expressed in the form of equation (II-16), the equilibrium function μ_i' becomes

$$\mu_i' = \frac{a}{1 + b\, y_i} \qquad \text{(A-2)}$$

For the case described in Sections II.2.2 and II.4.1, in which no chemical reaction exists, it was shown that μ_i' was equal to G*. In the limit, as y_i becomes very small, G* approaches a constant, a.

$$\lim_{y_i \to 0} G^* = a \qquad \text{(A-3)}$$

A.2 Dissociative Adsorption

Consider the alternative to Appendix A.1 in which the gas is diatomic and dissociates upon adsorption. The Langmuir equilibrium relation becomes

$$n_i' = \frac{a\, y_i^{1/2}}{1 + b\, y_i^{1/2}} \tag{A-4}$$

When expressed in the form of equation (II-16), the equilibrium function μ_i' becomes

$$\mu_i' = \frac{a\, y_i^{-1/2}}{1 + b\, y_i^{1/2}} \tag{A-5}$$

For the conditions referred to in Appendix A.1, G* was shown to be equal to μ_i'. Therefore, in the limit as y_i approaches zero, G* approaches infinity; that is,

$$\lim_{y_i \to 0} G^* = a y_i^{-1/2} \tag{A-6}$$

If G* is multiplied by $y_i^{1/2}$, the following limiting expression is obtained:

$$\lim_{y_i \to 0} G^*\, y_i^{1/2} = a \tag{A-7}$$

A.3 Freundlich Adsorption

A third type of adsorption isotherm is the Freundlich type. The Freundlich relationship is

$$n_i' = f y_i^{d} \tag{A-8}$$

where: f, d = constants at a given temperature.

When expressed in the form of equation (II-16), the equilibrium function μ_i' becomes

$$\mu_i' = f y_i^{d-1} \tag{A-9}$$

For the case described in Appendix A.1, G* was shown to be equal to μ_i'. Therefore G* becomes

$$G^* = f y_i^{d-1} \tag{A-10}$$

A.4 Relationship Between μ^B_{CO}, $\mu^B_{CO_2}$, and K_4'

The fact that only two of the above equilibrium constants are independent can be easily shown. Since

$$K_4' = \frac{n^B_{CO}}{n^B_{CO_2}} \tag{II-38d}$$

and

$$\mu^{B}_{CO} = \frac{n^{B}_{CO}}{y_{CO}} \qquad \text{(II-38b)}$$

$$\mu^{B}_{CO_2} = \frac{n^{B}_{CO_2}}{y_{CO_2}} \qquad \text{(II-38c)}$$

it follows that

$$K'_4 = \frac{\mu^{B}_{CO}\, y_{CO}}{\mu^{B}_{CO_2}\, y_{CO_2}} \qquad \text{(A-11)}$$

where the ratio $\frac{y_{CO}}{y_{CO_2}}$ was shown in Section II.2.3 to remain constant for a given carrier gas in the vicinity of the tracer.

APPENDIX B

MATERIALS

B.1 Helium, Argon

Helium and argon were both purchased in 1A cylinders. The helium was supplied by Iweco and had a stated minimum purity of 99.99%. The Matheson Company supplied the argon, which had a minimum purity of 99.995%.

B.2 Hydrogen

Hydrogen was purchased from the Matheson Company in a 1A cylinder. The Ultra High Purity grade had a purity of 99.999%.

B.3 Carbon Monoxide, Carbon Dioxide

Both carbon oxides were purchased from the Matheson Company in 1A cylinders at 99.5% minimum purity.

B.4 Radioactive Gases

The radioactive tracers were obtained from the New England Nuclear Company. Two millicuries of each, or a

total of four millicuries, were used throughout this work. The gases were shipped in glass ampoules containing one millicurie each. In the first shipment the specific activities of the carbon dioxide and the carbon monoxide were 30.8 and 4.5 millicuries per millimole, respectively. In the second shipment these respective values were 20.0 and 4.5.

B.5 Catalyst

The catalyst under study was Girdler G-66B Low Temperature CO Conversion catalyst, manufactured by the Catalysts Division of the Chemetron Corporation. The unreduced catalyst, consisting of copper oxide supported on zinc oxide, was received in the form of 1/4" x 1/8" pellets courtesy of Mr. Luis Guzman of Chemetron. The manufacturer listed the BET surface area as 25.4 m^2/g and Suzuki and Smith (49) experimentally determined it to be 35.9 m^2/g. These authors have presented a table of physical properties of this catalyst in both the unreduced and the reduced states based on their own investigation.

APPENDIX C

EXPERIMENTAL APPARATUS

C.1 Equipment Layout

The oven, temperature controller and heat source were all purchased in one integrated unit which stood approximately five feet high. A large metal stand was used to support the recorder, the electrometer, the thermal conductivity bridge and the D.C. power supply. Between the instrument stand and the oven was a large frame-like support constructed of slotted angle iron. Wooden shelves were placed in portions of this structure in order to support the preamplifier and the vacuum pump. The remainder of the equipment was mounted on the angle iron structure. The gas cylinders were clamped to this center support.

C.2 Tubing, Valves, Filters, Fittings

In general 1/8" type T Polypenco Nylaflow tubing was used. The primary advantage offered by this tubing was the ease of handling because of its flexibility and easy cutting. Because of the temperatures involved, stainless steel tubing was used to connect with the columns in the

oven. The sampling valve, test column, thermal conductivity cell and ionization chamber were connected by 1/8" x .042" stainless steel tubing. This size was selected in order to minimize dead volume in this region. The precolumn connecting tubing was also 1/8", but the wall thickness was .035" instead. The 1/16" tubing used in the construction of the bypass and the pressure taps is described elsewhere.

Swagelock fittings were used exclusively. Nearly all fittings were brass, although stainless steel was used on occasion.

Whitey OKS2 or ORS2 forged body valves were used almost exclusively. Exceptions were the two Whitey OGS2 toggle valves, a Whitey OKM2-S2A forged body valve used for tracer supply cutoff, and the metering valves.

C.3 Flow Control and Measurement

Flow control was provided by a constant differential type flow controller manufactured by the Moore Products Company. The specific model, 63BU-L, was constructed of brass and designed for low flow rates with a constant upstream pressure. The controller provided a constant pressure differential across a stainless steel Nupro very fine metering valve. Flow was varied by adjusting the metering valve.

Flow rates were measured by timing the displacement of soap bubbles in a 50 cc soap bubble meter. The timing device used was manufactured by the Precision Scientific Company and recorded time in tenths of a second.

C.4 Temperature Control and Measurement

The precolumn and the test column were thermostated in a Con-Wate Ultra-Temp oven, manufactured by the Blue-M Electric Company. Control to within 0.4°F was obtained over the short range, but over a period of days the temperature was observed to vary over a 5°F range. A temperature guard system was installed on the oven in order to prevent a temperature runaway resulting from a temperature controller malfunction.

For temperature measurement a chromel alumel thermocouple was positioned in the oven. The output was measured on a Leeds and Northrup model 8686 millivolt potentiometer.

In all, then, there were three thermocouples in this oven. One was for temperature control; another for temperature measurement; and the third for the runaway guard system.

C.5 Pressure Measurement

Pressure taps were installed inside the oven so that

once again stainless steel connecting tubing was employed. In keeping with the objective of minimizing dead volume, additional fittings were not incorporated for these pressure taps. Instead, 1/16" holes were tapped in the unions at the ends of both the short and the long columns (3 unions, since the columns were joined together), and lengths of 1/16" x .010" stainless steel tubing were silver soldered into place. Reducing unions (1/16" x 1/8") joined the 1/16" tubing to 1/8" tubing, which led directly to the three pressure gages. These Crosby gages measured pressures from 30" Hg vacuum to 15, 30 and 60 psig, respectively. Only two of these gages were really necessary. Therefore, the 60 psig gage was used only as a check on the other two gages.

C.6 Test Column and Precolumn

The precolumn was installed upstream of the test column in an attempt to remove any poisons in the carrier gas before reaching the test column. A 61.2 cm length of 3/8" x .035" stainless steel tubing was used to contain 39.3684 g of catalyst which had been ground and seived to a 35/48 Tyler mesh particle size range. Both ends of the column were fitted with glass wool plugs in order to hold the bed in place. A Mettler balance was used in all catalyst weighings.

The test column consisted of a long and a short column in series. As described previously, it was possible to use either the short column alone, or the two columns in series for experiments. Both columns were constructed of 1/4" x .035" stainless steel tubing. The short column contained 2.2671 g of 28/35 Tyler mesh catalyst and had a length of 10.0 cm. The long column was 101.4 cm long and contained 26.0905 g of 28/35 mesh catalyst. As with the precolumn, glass wool plugs were inserted in both columns. The two columns were connected by a 1/4" Swagelock union and wound into a helix. Two 1/16" holes were tapped in the side of this fitting in order to accomodate two lengths of 1/16" x .010" stainless steel tubing. These connections were silver soldered into place. One of these was a pressure tap, while the other was available to direct the carrier gas over the short column only when so desired. At the ends of the resulting test column Swagelock fittings were similarly tapped. As with the center fitting, one tap in each fitting was constructed for pressure measurement. A 2 1/2" section of 1/16" x .028" stainless steel capillary tubing was silver soldered into the remaining two holes in order to provide a partial bypass flow when the columns were operated in the combined mode. Proper proportioning of the flow between the bypass and the column could not be obtained <u>a priori</u> by selection of the appropriate inside

diameter. Therefore, it was necessary to flatten the bypass very slightly with a hammer until the desired bypass to column ratio could be approximated. Determination of the fraction of flow through the bypass is discussed in Appendix D.

A third 1/16" tap was provided at the short column exit. The 1/16" x .010" section of tubing, which was silver soldered in place, was connected to 1/8" x .042" tubing. This line was connected to one of the toggle valves and was used to generate a bypass peak when operating with the short column.

C.7 Sample System

The sample system is shown in Figure III-3. It consisted basically of a sample loop, sampling valve, pressure gage, vacuum source, tracer supply and connection tubing. The sampling valve was a standard two position six way chromatographic sampling valve. The sample loop had a volume of approximately 0.29 cc.

The stainless steel tubing in the manifold was 1/8" x .042", as every effort was made to minimize the dead volume and thus conserve the radioactive tracer. The pressure gage, manufactured by the Marsh Instrument Company, measured pressure from 30" Hg vacuum to 250 psig.

The system was designed so that not all the radioactive tracer would have to be diluted simultaneously. High vacuum stopcocks were joined to the glass ampoules in which the tracers were shipped while the breakseals remained unbroken. Kovar seals were joined to the other sides of the stopcocks in order to connect the assemblies to the Whitey valves, which in turn were connected to the manifold by Swagelock fittings. The space between the valve and the stopcock provided an excellent dilution volume, into which a portion of the tracer could be expanded and then diluted by the carrier gas, if necessary. In addition to these mixing volumes, a 30 cc Hoke 4HS30 sample cylinder was connected to the manifold. This container was used to hold some of the radioactive carbon monoxide which had been diluted with mixture 1.

It was felt that by employing the high vacuum stopcocks and the original glass ampoules better protection against air contamination could be achieved than by methods used by previous investigators.

C.8 Thermal Conductivity System

The thermal conductivity cell was used to measure concentration disturbances in the gas exiting the column. In free volume determinations argon peaks were monitored

as the helium carrier gas swept the sample through the cell. In experiments involving the carbon oxide mixtures as carrier gases, the thermal conductivity system was used to determine if the chromatographic system was at equilibrium before a sample was injected. Concentration peaks were not used in chemisorption analysis because of small amplitude and variable polarity.

The thermal conductivity system is shown in Figure C-1. The cell was a Gow-Mac model 133 micro-thermal conductivity cell. It was constructed of stainless steel and had an internal volume of 0.115 cc. Detection was provided by a matched pair of 8K ohm glass bead thermistors mounted inside the cell. The response time was stated by the manufacturer to be less than 0.5 second. The assembly was mounted on a wood support and no attempt was made to insulate the cell from ambient conditions.

The thermistors were an integral part of a standard wheatstone bridge assembly, which in this case was a home-made device. The D.C. power supply was a Kepco model ABC 75-2. The device was set at 7.5 volts throughout this study, and bridge currents of approximately 3 milliamperes were typical. The bridge output was connected to the recorder channel which was equipped with the integrator.

Numerical Legend

Figure C-1

1. D.C. Power Supply
2. Bridge Assembly
3. Recorder
4. Thermistor Mounting
5. Thermal Conductivity Cell
6. Flow From Precolumn
7. Flow From Test Column

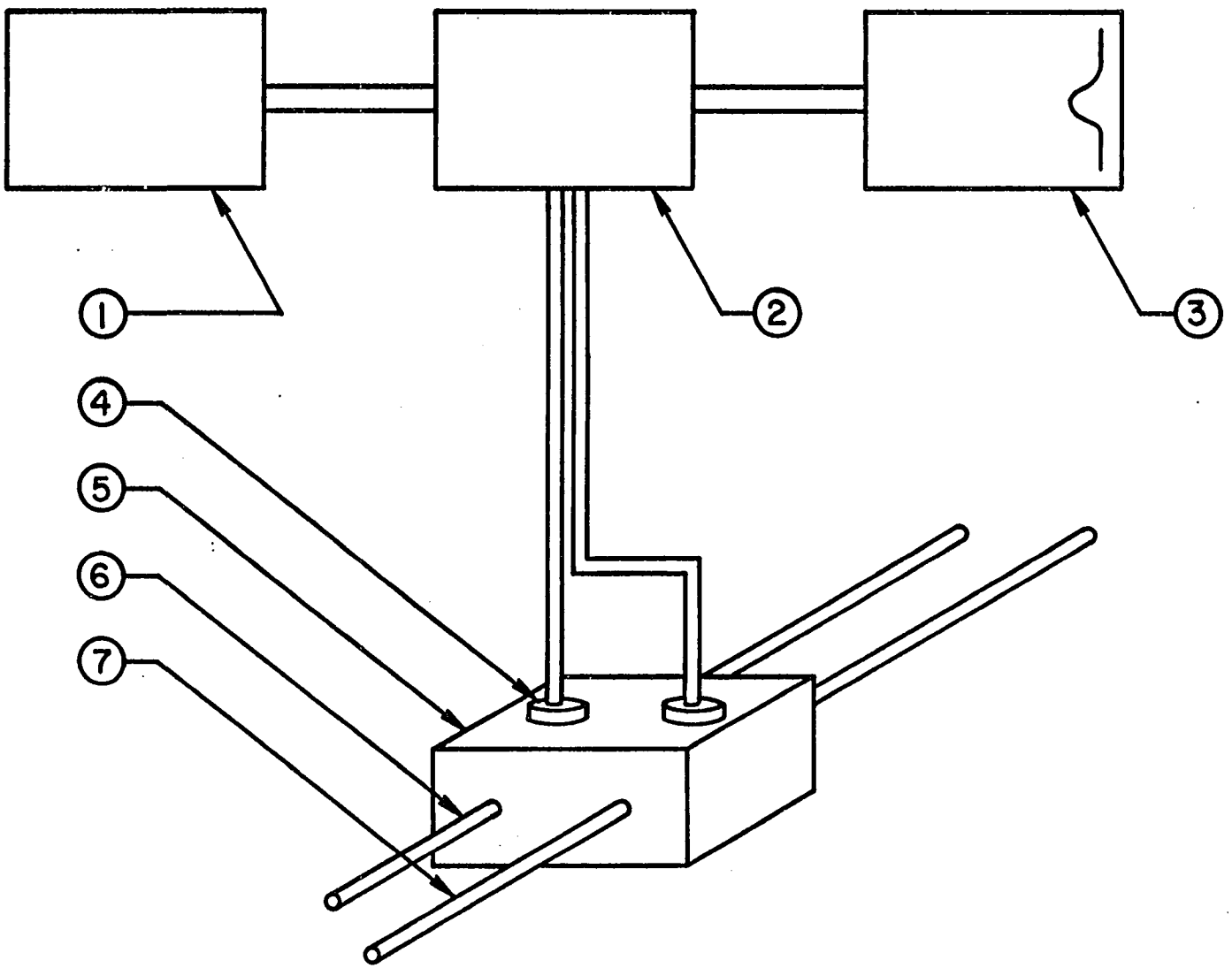

FIGURE C-1 THERMAL CONDUCTIVITY DETECTION SYSTEM

C.9 Radioactive Detection System

The eluted radioactive sample was detected in a 3 cc stainless steel ionization chamber. Figure C-2 shows the chamber, along with a schematic diagram of the radioactive detection system. The chamber was designed specifically for this type of service and had been used previously by other investigators. The outer wall of the chamber served as one electrode, while a 1/8" polished stainless steel rod in the center of the chamber served as the other. A six volt potential, supplied by four 1.5 volt Burgess dry cells connected in series, was placed across these electrodes. The center electrode was insulated from the chamber by Kel-F. Care had to be taken to insure that this Kel-F spacer remained clean. On several occasions water and fine catalyst particles contaminated the insulator during the activation process. Inability to zero the electrometer resulted.

As the radioactive molecules enter the detector, the energy released during the decay process ionizes some of the surrounding gas molecules. The ions are caught in the resulting field and migrate to the appropriate electrodes. A small current, which is proportional to the level of radioactivity in the chamber, results. Currents of the order of 10^{-14} amperes were typical in this work. The preamplifier was connected to the Model 401 Cary Vibrating

Numerical Legend

Figure C-2

1. 1/8" Nylon Tubing
2. S S Connector
3. Ionization Chamber
4. Preamplifier
5. Electrometer
6. Recorder
7. 6 Volt Dry Cell
8. S S
9. Kel-F
10. Brass
11. Brass Adapter
12. Teflon

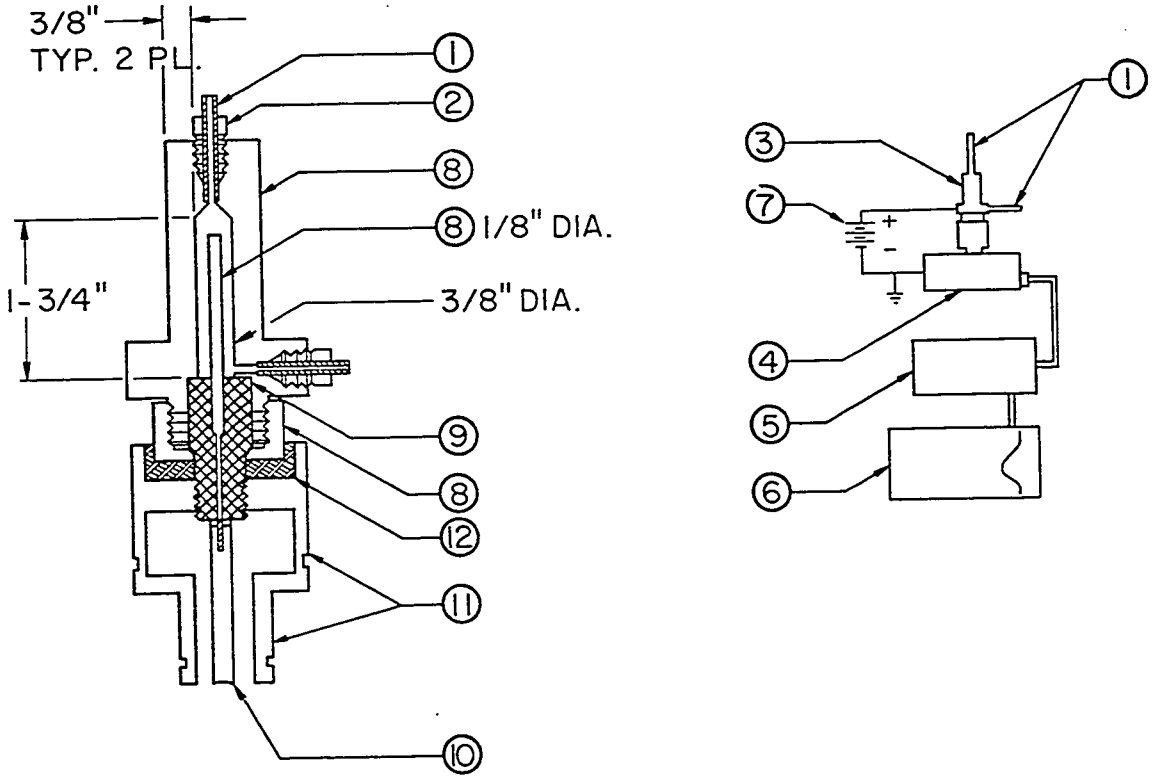

FIGURE C-2 RADIOACTIVE DETECTION SYSTEM

Reed Electrometer by a four foot coaxial cable. The electrometer was operated with the resistor set at 10^{12} ohms. The preamplifier was in the critical damping mode. The output of the electrometer was fed to the recorder for simultaneous monitoring with the thermal conductivity output. Operation in the critical damping mode resulted in a response time of approximately 1 second.

C.10 Recorder

Both the thermal conductivity cell and the ionization chamber responses were recorded on a Hewlett-Packard Model 7100B two channel recorder. One channel, the thermal conductivity channel, was provided with an integrator. The instrument was capable of measuring voltages varying from 1 millivolt to 100 volts. The chart speed could be varied from 1 inch per hour to 2 inches per second.

C.11 Vacuum Pump

A Welch Duo-Seal vacuum pump was used to evacuate the sample manifold and portions of the flow system. Normally a 29" Hg vacuum was obtained.

APPENDIX D

EXPERIMENTAL PROCEDURE DETAILS

D.1 Catalyst Preparation and Activation

The catalyst was ground and sieved to 28/35 and 35/48 Tyler mesh fractions. The smaller particle size was used in the precolumn. The tubing was cut to the appropriate length, washed with acetone, and dried in a stream of nitrogen. A 1/8"-1/4" glass wool plug was placed in one end. The tubing was then secured by a clamp on a ringstand and held in a verticle position. Catalyst from a preweighed vial was then poured into the column through a funnel until the level rose to within 1/4" of the top. All the while the column was vigorously tapped in order to maximize packing. The top end was plugged with glass wool before installation in the oven. The vial was then reweighed and the weight of the catalyst in the column determined by difference. All three columns were prepared in this manner. The precolumn was installed and the long and short columns were connected in the series configuration.

The activation procedure was essentially the same as those used by Musser (38) and recommended by the

manufacturer. The helium flow rate was first established at approximately 3.7 cc/sec, ambient conditions. Hydrogen flow was then combined with the helium flow at such a rate as to result in a 1% hydrogen mixture. Simultaneously the oven was set at 400°F. Condensation could be observed in the exit lines shortly thereafter, indicating that reduction was taking place. After six hours the hydrogen flow was increased to give a 2% mixture. After a second six hour period the hydrogen level was increased to 5%. At the end of the final six hour period the flow of hydrogen was terminated, and the helium flow was reduced in preparation for the free volume and bypass calibration procedures. It was necessary to know, of course, the proper hydrogen metering valve settings before activation was started.

The activation step apparently was reproducible from one column to another. In some preliminary work which led to the work described in this thesis, a different column was prepared and activated by the same procedure described above. Adsorption data with mixture 1 gave results which were identical, within experimental error, to results from columns discussed herein.

A check on the catalyst activity with respect to time was accomplished by comparing the level of adsorption with a mixture 1 carrier gas at a given flow rate. The

first check was carried out upon the completion of experiments with mixtures 1, 2 and 3. It showed only slight, if any, deactivation. After work with mixtures 4, 5 and 6 was finished, a second check was made. In this case the activity had decreased to approximately 84% of the original level. After mixture 7 experiments were completed, a final check showed that about 17% of the activity had been lost. These check points are shown in Figure IV-1.

D.2 Carrier Gas Mixtures

A mixing manifold was constructed to facilitate preparation of the carrier gas mixtures. The valves were Whitey OKS4 stainless steel forged body valves. The connecting tubing was 1/4" x .035" stainless steel. A Heise 0-1000 psia gage was used to measure the pressure as the gases were expanded into a previously evacuated 1A gas cylinder. The mixing cylinder was actually purged with one of the carbon oxides and evacuated three times. Each gas was slowly expanded from its supply into the mixing cylinder until the desired pressure was attained.

Final compositon analysis of the carbon monoxide-carbon dioxide mixtures was made on a Consolidated Electrodynamics Type 21-104 mass spectrometer. Carbon dioxide-helium mixture compositions were determined by pressure

measurements before and after freezing the carbon dioxide in a vacuum system. The mixtures used in this work, along with their compositions are listed in Table D-1.

TABLE D-1 Carrier Gas Compositions

Mixture	Vol. % He	Vol. % CO_2	Vol. % CO
1	0.0	93.5	6.5
2	0.0	72.4	27.6
3	0.0	36.5	63.5
4	0.0	99.6	0.4
5	0.0	5.3	94.7
6	0.0	0.0	100.0
7	0.0	100.0	0.0
8	92.7	7.3	0.0
9	71.1	28.9	0.0
10	85.8	14.2	0.0
11	90.0	10.0	0.0
12	92.8	7.2	0.0
13	87.6	12.4	0.0

D.3 Radioactive Sample Preparation

A physical description of the sample manifold is presented in Appendix C. When the stopcock was joined to

the ampoule containing the tracer, a ball bearing was placed in a specially prepared pocket. The ball bearing was therefore held above and slightly to the side of the breakseal. The valves and the stopcock were positioned in such a way as to evacuate the sample manifold up to the breakseal. When the vacuum was deemed satisfactory, the stopcock was closed. A magnet was used to dislodge the ball bearing and cause it to fall on the breakseal. Several attempts were required because of the short distance of fall and the light weight of the ball bearing. When the seal was broken, the tracer was ready for use. Both tracer supplies were prepared for use in this manner.

A large amount of carbon monoxide tracer was expanded into the 30 cc sample container. The tracer in this container was then diluted by the addition of mixture 1. From these supplies samples could be diluted and expanded as necessary for injection.

D.4 Free Volume Calibration

For both the long and short columns free volume calibrations were made in order to determine the void volumes of the columns. From the free volume and the flow data, the carrier gas residence time, t_r, in the column could be calculated. The free volume, V_G, can be expressed as

$$V_G = Q\ t_r \qquad \text{(D-1)}$$

Experimentally this determination was accomplished by injecting argon samples into a helium carrier stream. Argon, of course, does not adsorb and therefore travels through the column at the same velocity as the carrier gas. For the short column, two samples were required in order to determine a value for t_r. This procedure is described under Section III.2. For the long column, only one sample was required since one sample resulted in bypass and main column peaks. After correcting the measured flow rates to column conditions to obtain Q, V_G could be determined by equation (D-1).

For the short column the average free volume, V_G, was 1.86 cc. The value of V_G for the long column was 16.8 cc. The data and calculated results for these determinations are presented in Appendices G and H, respectively.

D.5 Bypass Line Calibration

When the bypass was used it was necessary to know what portion of the flow approaching the column was diverted by the column. This was determined at the same time the free volume calibration was carried out. Since the thermal conductivity cell output was connected to the recorder

channel with the integrator, the areas of the peaks were known. The fraction of flow bypassing the column could be calculated by the following expression:

$$f_B = \frac{\text{area of bypass peak}}{\text{area of bypass peak + area of main peak}}$$

It was assumed that the thermal conductivity cell response was proportional to the argon concentration. This assumption was verified experimentally for the range of argon concentrations used.

When the columns were in series, 22.9% of the flow bypassed the column. As with free volume determinations results from a number of runs were averaged. The experimental f_B values are included with the free volume data in Appendix G.

D.6 Peak Analysis

The determination of the residence time of a sample in a column from a chromatogram can sometimes not be a straightforward task. Strictly speaking, graphical integration should be carried out in order to determine the centroid of the peak. In this work, however, this method was rendered useless because of the excessive tailing, which introduces large amounts of error into this procedure.

Selecting the peak maximum provided the easiest approach. This was totally satisfactory with the argon-helium data because of the smoothness of the peaks. However, with the radioactive peaks this method proved unreliable because of the stochastic nature of these peaks. The problem was finally resolved by the following procedure. A line was drawn through the peak parallel to the baseline at an amplitude equal to 50% of the maximum value. The segment of this line situated within the peak then was bisected. This point, then, represented the time reference point of the peak. The method showed good reproducibility. The data showed considerably less scatter when this method was used instead of attempting to locate the peak maximum.

APPENDIX E

SAMPLE CALCULATIONS

E.1 The average column pressure, P_c, was calculated for every run from the three pressure readings recorded as data.

$$P_c = \frac{P_i + P_o}{2} + P_a$$

$$P_c = \frac{(2.9 + 0.0)}{2} \text{ psig} \cdot 51.71 \frac{\text{mm}}{\text{psig}} + 30.520 \text{ in Hg} \cdot 25.4 \frac{\text{mm}}{\text{in}}$$

$$P_c = 852.8 \text{ mm Hg}$$

E.2 The column flow rate, Q, was calculated from the measured flow rate as follows:

$$Q = Q_m \cdot \frac{P_a}{P_c} \cdot \frac{T_c}{T_r} \cdot \left(1 - \frac{P_{H_2O}}{P_a}\right) \cdot (1 - f_B)$$

$$Q = 1.0860 \frac{\text{cc}}{\text{sec}} \cdot \frac{775.2 \text{ mm}}{852.8 \text{ mm}} \cdot \frac{477.9 \text{ °K}}{296.3 \text{ °K}} \cdot \left(1 - \frac{21.196 \text{ mm}}{775.2 \text{ mm}}\right) \cdot (1 - .229)$$

$$Q = 1.1943 \frac{cc}{sec}$$

For the short column, $f_B = 0$.

E.3 The column free gas volume, V_G, was calculated from the argon - helium data as follows:

$$V_G = Q \cdot t_r, \quad \text{where } t_r = t_p \text{ for argon.}$$

$$V_G = 0.2331 \frac{cc}{sec} \cdot 72.0 \text{ sec}$$

For the long column, V_G values for various runs were averaged.

$$V_G = \frac{(17.05+17.00+17.00+17.00+16.64+16.78+16.92+16.57+16.66+16.57)}{10}$$

$$V_G = 16.8 \text{ cc}$$

For the short column, one average residence time was determined for each of three flow rates with the corresponding V_G values subsequently being calculated. These latter values were then averaged.

$$V_G = \frac{1.898 + 1.867 + 1.829}{3}$$

$V_G = 1.86$ cc

E.4 The fraction of flow going through the bypass, f_B, was calculated as follows from the argon - helium data:

$$f_B = \frac{A_B}{A_B + A_C}$$

$$f_B = \frac{1.36}{1.36 + 4.55}$$

$$f_B = 0.230$$

The individual determinations were then averaged.

$$f_B = \frac{.232+.230+.226+.223+.228+.231+.231+.228+.232+.229}{10}$$

$$f_B = 0.229$$

E.5 The residence time of the carrier gas flowing through the column, t_r, could then be calculated as follows:

$$t_r = \frac{V_G}{Q}$$

$$t_r = \frac{16.8 \text{ cc}}{1.194 \text{ cc/sec}}$$

$$t_r = 14.1 \text{ sec}$$

E.6 The peak residence times were calculated differently depending on which column was in use. For the long column the following procedure was followed:

$$t_p = L_r \cdot \frac{1}{C_s}$$

$$t_p = 2.15 \text{ in} \cdot \frac{1}{2 \text{ in/min}} \cdot 60 \text{ sec/min}$$

$$t_p = 64.5 \text{ sec}$$

The peak residence time in the short column was calculated as follows:

$$t_p = L_{r1} \cdot 1/C_{s1} - L_{r2} \cdot 1/C_{s2}$$

$$t_p = 4.43 \text{ in} \cdot 1/(2 \text{ in/sec}) - 2.16 \text{ in} \cdot 1/(2 \text{ in/sec})$$

$$t_p = 1.14 \text{ sec}$$

E.7 The column conversion constant, β, was calculated as follows:

$$\beta = \frac{m}{V_G c}, \quad \text{where } c = \frac{P_c}{R\,T_c}$$

$$c = 852.8 \text{ mm}/\left(62360 \frac{\text{mm cc}}{\text{g mole°K}} \cdot 477.9°\text{K}\right)$$

$$c = 2.862 \cdot 10^{-5} \text{ g mole/cc}$$

$$\beta = \frac{28.3576 \text{ g catalyst}}{16.8 \text{ cc} \cdot 2.862 \cdot 10^{-5} \text{ g mole/cc}}$$

$$\beta = 5.899 \cdot 10^{4} \text{ g catalyst/g mole}$$

E.8 G* was then calculated according to the equation

$$G^* = \frac{1}{\beta} \cdot (t_p/t_r - 1)$$

$$G^* = \frac{1}{5.899 \cdot 10^{4}} \cdot (64.5/14.1 - 1)$$

$$G^* = 6.059 \cdot 10^{-5} \text{ g mole/g catalyst .}$$

APPENDIX F

ERROR ANALYSIS

F.1 Temperature

A 0.2°C graduated mercury thermometer was used to measure the room temperature to within ± 0.1 °C. For a room temperature of 23°C, the error in T_r is ± (0.1) (100)/ 296 = ±0.034%.

The short term fluctuation of the column temperature, T_c, was less than ±0.2°C. The resulting error in T_c is ±(0.2) (100)/477 = ±0.042%.

F.2 Pressure

The atmospheric pressure was measured to within ±0.005 inches of mercury. The error in P_a is ±(.005) (100)/ 30 = ±0.017%.

The inlet pressure was measured on a gage which could be read to an accuracy of ±0.05 psi. For an inlet pressure of 2 psig the resulting error in P_i is ±(.05)(100)/ 16.7 = ±0.30%.

The same degree of accuracy was obtained for the outlet pressure gage, and the resulting error in P_o for an

outlet pressure of ±0.5 psig is ±(.05)(100/15.2 = ±0.33%.

The average column pressure was calculated by the formula $P_c = \frac{P_i + P_o}{2} + P_a$. For an average pressure of 820 mm, the error in P_c is ±((.30 + .33)/2 + .017) = ±0.33%.

F.3 Time and Distance

Distance measurements on recorder charts were made to within ±(.01)(100)/2 = ±0.5%.

A stopwatch graduated in tenths of a second was used to measure time elapsed in recording flow rates with the bubble meter. Repeated measurements were reproducible to within ±0.3 sec for a 100 sec time interval. The resulting error in the measured flow rate, Q_m, is ±(0.3)(100)/100 = ±0.3%.

F.4 Column Flow Rate

The column flow rate is given by

$$Q = Q_m \cdot (P_a/P_c) \cdot T_c/T_r, \cdot \left(1 - \frac{P_{H_2O}}{P_a}\right) \cdot (1-f_B).$$

The resulting error in Q is ±(.30 + .33 + .078 + .024 + .27) = ±1.0%.

F.5 Catalyst Weight

The catalyst was weighed on a Mettler balance to an accuracy of ±0.0001 g. But due to the handling procedure in packing the columns it is doubtful that the weight of the catalyst, m, was known to limits better than ±0.001 g. For the short column this results in an error of ±(.001)(100)/2.2671 = ±0.044%.

For the long column the error in m is (.001)(100)/28.3576 = ±0.004%.

F.6 Bypass Fraction

The peak areas, A_C and A_B, used in calculating the fraction of flow which bypassed the column could be determined to within ±0.01. For a typical determination, in which A_C = 4.55 and A_B = 1.36, the resulting error in f_B = ±(.0021)(100)/0.230 = ±0.91%.

F.7 Column Free Volume

The column free volume, V_G, was determined by the product $Q \cdot t_p$, where the t_p referred to the residence time of an argon sample in a helium carrier gas. The error in V_G is therefore = ±(1.0 + 0.5) = ±1.5%.

F.8 Column Conversion Constant

The column conversion constant, β, was determined by the expression, $\beta = \frac{m}{V_G C}$. When the ideal gas law is assumed, this becomes $\beta = \frac{mRT_c}{V_G P_c}$. The error in this term then is = $\pm(.044 + .042 + .33 + 1.5) = \pm 1.92\%$.

F.9 G* Error

The resulting error in G*, calculated by $(1/\beta)(t_p/t_r - 1)$, is $\pm(1.92 + 3.85) = \pm 5.77\%$.

APPENDIX G

RAW DATA

RAW DATA - MIXTURE 1

6.5 % CO

93.5 % CO2

COLUMN	TOTAL FLOW RATE, CC/SEC	TR, DEG C	TC, DEG C	PA, IN HG	PI, PSIG	PO, PSIG	SAMPLE	RET TIME, SEC
SHORT	4.5714	23.9	203.6	30.485	3.00	0.55	C140	1.70
SHORT	4.5714	23.9	203.6	30.485	3.00	0.55	C1402	0.45
SHORT	3.5336	24.0	204.1	30.482	2.20	0.40	C140	2.19
SHORT	3.5336	24.0	204.1	30.482	2.20	0.40	C1402	0.66
SHORT	2.7045	23.8	204.0	30.500	1.70	0.30	C140	2.85
SHORT	2.7045	23.8	204.0	30.500	1.70	0.30	C1402	0.78
SHORT	1.8575	23.1	203.9	30.532	1.30	0.20	C140	3.84
SHORT	1.8575	23.1	203.9	30.532	1.30	0.20	C1402	1.01
SHORT	1.0743	23.2	203.9	30.538	0.60	0.10	C140	6.39
SHORT	1.0743	23.2	203.9	30.538	0.60	0.10	C1402	1.95
SHORT	0.7304	24.0	204.0	30.487	0.50	0.05	C140	9.24
SHORT	0.7304	24.0	204.0	30.487	0.50	0.05	C1402	2.73
SHORT	0.4275	24.0	204.0	30.486	0.40	0.05	C140	15.10
SHORT	0.4275	24.0	204.0	30.486	0.40	0.05	C1402	5.10
SHORT	0.3128	23.2	203.9	30.542	0.30	0.00	C140	19.67
SHORT	0.3128	23.2	203.9	30.542	0.30	0.00	C1402	7.40
SHORT	0.2031	23.6	203.8	30.490	0.20	0.00	C140	27.80
SHORT	0.2031	23.6	203.8	30.490	0.20	0.00	C1402	13.40
SHORT	0.1232	23.5	203.7	30.492	0.20	0.00	C140	42.00
SHORT	0.1232	23.5	203.7	30.492	0.20	0.00	C1402	24.00
SHORT	0.0789	23.2	204.6	30.550	0.00	0.00	C140	67.05
SHORT	0.0789	23.2	204.6	30.550	0.00	0.00	C1402	53.10
LONG	1.0860	23.1	204.8	30.520	2.90	0.10	C140	64.50
LONG	1.0860	23.1	204.8	30.520	2.90	0.10	C140	63.90
LONG	1.0860	23.1	204.8	30.520	2.90	0.10	C1402	42.60
LONG	0.6438	23.7	204.9	30.522	1.80	0.05	C140	97.20
LONG	0.6438	23.7	204.9	30.522	1.80	0.05	C1402	85.20
LONG	0.3275	24.0	204.8	30.512	1.00	0.05	C140	201.60
LONG	0.3275	24.0	204.8	30.512	1.00	0.05	C1402	189.60
LONG	0.1643	24.0	204.5	30.500	0.55	0.00	C140	436.80
LONG	0.1643	24.0	204.5	30.500	0.55	0.00	C1402	429.60
LONG	0.0828	24.0	204.3	30.476	0.35	0.00	C140	942.00
LONG	0.0828	24.0	204.3	30.476	0.35	0.00	C1402	942.00

RAW DATA - MIXTURE 2

27.6 % CO

72.4 % CO2

COLUMN	TOTAL FLOW RATE, CC/SEC	TR, DEG C	TC, DEG C	PA, IN HG	PI, PSIG	PO, PSIG	SAMPLE	RET TIME, SEC
SHORT	4.5249	23.8	203.3	30.090	2.80	0.55	C140	1.19
SHORT	4.5249	23.8	203.3	30.090	2.80	0.55	C1402	0.49
SHORT	3.0918	24.0	203.4	30.117	1.95	0.35	C140	1.83
SHORT	3.0918	24.0	203.4	30.117	1.95	0.35	C1402	0.55
SHORT	2.5668	24.0	203.4	30.124	1.60	0.30	C140	2.24
SHORT	2.5668	24.0	203.4	30.124	1.60	0.30	C1402	0.79
SHORT	1.6937	24.0	203.6	30.132	1.10	0.20	C140	3.24
SHORT	1.6937	24.0	203.6	30.132	1.10	0.20	C1402	1.15
SHORT	1.0582	24.0	203.6	30.138	0.70	0.10	C140	5.03
SHORT	1.0582	24.0	203.6	30.138	0.70	0.10	C1402	1.68
SHORT	0.7326	23.9	203.4	30.090	0.50	0.05	C140	7.36
SHORT	0.7326	23.9	203.4	30.090	0.50	0.05	C1402	2.64
SHORT	0.4324	23.9	203.3	30.100	0.35	0.05	C140	12.30
SHORT	0.4324	23.9	203.3	31.000	0.35	0.05	C1402	4.92
SHORT	0.3200	24.0	203.6	30.150	0.30	0.00	C140	16.15
SHORT	0.3200	24.0	203.6	30.150	0.30	0.00	C1402	7.00
SHORT	0.1939	23.8	203.3	30.088	0.20	0.00	C140	25.80
SHORT	0.1939	23.8	203.3	30.088	0.20	0.00	C1402	12.10
SHORT	0.1177	23.8	203.3	30.099	0.20	0.00	C140	41.85
SHORT	0.1177	23.8	203.3	30.099	0.20	0.00	C1402	25.35
SHORT	0.0780	24.0	203.6	30.158	0.10	0.00	C140	64.20
SHORT	0.0780	24.0	203.6	30.158	0.10	0.00	C1402	48.70
LONG	1.0526	23.8	203.9	30.225	2.90	0.10	C140	73.50
LONG	1.0526	23.8	203.9	30.225	2.90	0.10	C1402	44.40
LONG	0.6808	23.8	203.9	30.215	2.00	0.05	C140	95.40
LONG	0.6808	23.8	203.9	30.215	2.00	0.05	C1402	76.20
LONG	0.3243	24.0	203.6	30.093	1.00	0.00	C140	199.20
LONG	0.3236	23.8	203.6	30.214	1.00	0.00	C140	196.80
LONG	0.3236	23.8	203.6	30.214	1.00	0.00	C1402	201.60
LONG	0.1559	23.9	203.6	30.189	0.60	0.00	C140	459.60
LONG	0.1559	23.9	203.6	30.189	0.60	0.00	C1402	474.00
LONG	0.0763	24.0	203.5	30.138	0.30	0.00	C140	1053.00
LONG	0.0763	24.0	203.5	30.138	0.30	0.00	C1402	1077.00

RAW DATA - MIXTURE 3

63,5 % CO

36,5 % CO2

COLUMN	TOTAL FLOW RATE, CC/SEC	TR, DEG C	TC, DEG C	PA, IN HG	PI, PSIG	PO, PSIG	SAMPLE	RET TIME, SEC
SHORT	4,8115	22,6	205,8	30,035	3,10	0,60	C140	0,66
SHORT	4,8115	22,6	205,8	30,035	3,10	0,60	C1402	0,63
SHORT	3,2154	22,9	205,9	30,079	2,10	0,40	C140	1,00
SHORT	3,2154	22,9	205,9	30,079	2,10	0,40	C1402	0,76
SHORT	2,6534	23,0	206,1	30,087	1,80	0,30	C140	0,96
SHORT	2,6534	23,0	206,1	30,087	1,80	0,30	C1402	0,77
SHORT	1,8363	23,0	206,0	30,094	1,30	0,20	C140	1,61
SHORT	1,8363	23,0	206,0	30,094	1,30	0,20	C1402	1,01
SHORT	1,0453	23,0	205,9	30,094	0,75	0,10	C140	2,61
SHORT	1,0453	23,0	205,9	30,094	0,75	0,10	C1402	1,71
SHORT	0,5423	23,0	205,9	30,097	0,45	0,05	C140	4,94
SHORT	0,5423	23,0	205,9	30,097	0,45	0,05	C1402	4,32
SHORT	0,3041	23,0	205,9	30,092	0,35	0,00	C140	8,90
SHORT	0,3041	23,0	205,9	30,092	0,35	0,00	C1402	7,70
SHORT	0,1411	23,0	206,3	30,083	0,20	0,00	C140	18,60
SHORT	0,1411	23,0	206,3	30,083	0,20	0,00	C1402	19,80
SHORT	0,0640	22,5	206,0	30,078	0,15	0,00	C140	44,10
SHORT	0,0640	22,5	206,0	30,078	0,15	0,00	C1402	54,90
LONG	1,0283	23,2	205,9	30,141	2,90	0,10	C140	39,00
LONG	1,0283	23,2	205,9	30,141	2,90	0,10	C140	39,00
LONG	1,0283	23,2	205,9	30,141	2,90	0,10	C1402	33,90
LONG	0,5502	23,1	206,0	30,150	1,70	0,50	C140	70,80
LONG	0,5502	23,1	206,0	30,150	1,70	0,50	C1402	70,80
LONG	0,2954	23,0	206,1	30,152	0,95	0,00	C140	129,60
LONG	0,2954	23,0	206,1	30,152	0,95	0,00	C1402	133,20
LONG	0,1491	22,8	206,5	30,139	0,55	0,00	C140	266,40
LONG	0,1491	22,8	206,5	30,139	0,55	0,00	C1402	306,00
LONG	0,0626	22,3	206,7	30,090	0,30	0,00	C140	1188,00
LONG	0,0626	22,3	206,7	30,090	0,30	0,00	C1402	1323,00

RAW DATA - MIXTURE 4

0.4 % CO

99.6 % CO2

COLUMN	TOTAL FLOW RATE, CC/SEC	TR, DEG C	TC, DEG C	PA, IN HG	PI, PSIG	PO, PSIG	SAMPLE	RET TIME, SEC
SHORT	4.6948	20.9	203.9	30.680	2.90	0.55	C140	1.35
SHORT	4.6948	20.9	203.9	30.680	2.90	0.55	C1402	0.73
SHORT	3.7951	21.0	204.0	30.680	2.40	0.40	C140	1.85
SHORT	3.7951	21.0	204.0	30.680	2.40	0.40	C140	1.30
SHORT	3.7951	21.0	204.0	30.680	2.40	0.40	C1402	0.66
SHORT	2.6774	21.0	203.9	30.679	1.70	0.30	C140	0.92
SHORT	2.6774	21.0	203.9	30.679	1.70	0.30	C140	1.11
SHORT	2.6774	21.0	203.9	30.679	1.70	0.30	C1402	0.92
SHORT	2.6774	21.0	203.9	30.679	1.70	0.30	C1402	0.87
SHORT	1.8045	20.8	204.0	30.683	1.20	0.20	C140	1.31
SHORT	1.8045	20.8	204.0	30.683	1.20	0.20	C1402	1.29
SHORT	1.8045	20.8	204.0	30.683	1.20	0.20	C1402	1.26
SHORT	1.0613	21.0	204.0	30.680	0.80	0.10	C140	1.97
SHORT	1.0613	21.0	204.0	30.680	0.80	0.10	C1402	1.74
SHORT	0.5587	20.9	204.1	30.682	0.50	0.05	C140	3.64
SHORT	0.5587	20.9	204.1	30.682	0.50	0.05	C1402	3.66
SHORT	0.5587	20.9	204.1	30.682	0.50	0.05	C1402	3.78
SHORT	0.3151	21.0	204.1	30.676	0.30	0.05	C140	8.67
SHORT	0.3151	21.0	204.1	30.676	0.30	0.05	C1402	8.22
LONG	0.5574	21.0	203.8	30.700	1.55	0.05	C140	85.20
LONG	0.5574	21.0	203.8	30.700	1.55	0.05	C1402	85.80
LONG	0.3161	21.0	205.7	30.719	0.95	0.05	C140	168.00
LONG	0.3161	21.0	205.7	30.719	0.95	0.05	C1402	168.00
LONG	0.1616	21.1	203.9	30.692	0.55	0.00	C140	364.80
LONG	0.1616	21.1	203.9	30.692	0.55	0.00	C1402	361.20
LONG	0.0627	21.5	205.3	30.769	0.20	0.00	C140	1069.20
LONG	0.0627	21.5	205.3	30.769	0.20	0.00	C1402	1086.00

RAW DATA - MIXTURE 5

94.7 % CO

5.3 % CO2

COLUMN	TOTAL FLOW RATE, CC/SEC	TR, DEG C	TC, DEG C	PA, IN HG	PI, PSIG	PO, PSIG	SAMPLE	RET TIME, SEC
SHORT	5.3262	22.0	203.4	30.306	3.30	0.65	C140	0.32
SHORT	5.3262	22.0	203.4	30.306	3.30	0.65	C1402	1.75
SHORT	3.3076	22.0	203.8	30.306	2.10	0.40	C140	0.52
SHORT	3.3076	22.0	203.8	30.306	2.10	0.40	C1402	2.22
SHORT	2.8090	22.0	203.8	30.305	1.80	0.30	C140	0.85
SHORT	2.8090	22.0	203.8	30.305	1.80	0.30	C1402	3.16
SHORT	1.6461	22.0	205.2	30.294	1.10	0.15	C140	1.27
SHORT	1.6461	22.0	205.2	30.294	1.10	0.15	C1402	4.77
SHORT	0.9424	21.7	205.2	30.299	0.70	0.10	C140	2.38
SHORT	0.9424	21.7	205.2	30.299	0.70	0.10	C1402	7.90
SHORT	0.5868	22.3	204.5	30.268	0.50	0.10	C140	3.72
SHORT	0.5868	22.3	204.5	30.268	0.50	0.10	C1402	12.28
SHORT	0.5868	22.3	204.5	30.268	0.50	0.10	C1402	12.64
SHORT	0.2883	22.3	204.5	30.268	0.35	0.05	C140	8.00
SHORT	0.2883	22.3	204.5	30.268	0.35	0.05	C1402	19.35
SHORT	0.1762	22.4	204.5	30.251	0.20	0.05	C140	15.00
SHORT	0.1762	22.4	204.5	30.251	0.20	0.05	C1402	27.60
LONG	0.5413	22.0	203.0	30.279	1.70	0.05	C140	60.60
LONG	0.5413	22.0	203.0	30.279	1.70	0.05	C1402	67.20
LONG	0.2925	21.9	204.6	30.215	1.00	0.05	C140	109.20
LONG	0.2925	21.9	204.6	30.215	1.00	0.05	C1402	122.40
LONG	0.1361	22.0	204.6	30.218	0.50	0.00	C140	237.60
LONG	0.1361	22.0	204.6	30.218	0.50	0.00	C1402	261.60
LONG	0.0739	22.0	202.9	30.251	0.40	0.00	C140	462.00
LONG	0.0739	22.0	202.9	30.251	0.40	0.00	C1402	492.00

RAW DATA - MIXTURE 6

100.0 % CO

0.0 % CO2

COLUMN	TOTAL FLOW RATE, CC/SEC	TR, DEG C	TC, DEG C	PA, IN HG	PI, PSIG	PD, PSIG	SAMPLE	RET TIME, SEC
SHORT	4.2735	22.3	205.6	29.977	2.70	0.55	C140	0.19
SHORT	2.7663	23.3	204.4	29.929	1.85	0.35	C140	0.87
SHORT	2.7663	23.3	204.4	29.929	1.85	0.35	C1402	11.49
SHORT	2.3041	23.4	204.6	29.935	1.55	0.30	C140	0.91
SHORT	2.3041	23.4	204.6	29.935	1.55	0.30	C1402	5.85
SHORT	1.3514	23.1	204.0	29.977	0.95	0.15	C140	1.57
SHORT	1.3514	23.1	204.0	29.977	0.95	0.15	C1402	12.13
SHORT	0.8011	23.1	204.0	29.986	0.55	0.10	C140	2.77
SHORT	0.8011	23.1	204.0	29.986	0.55	0.10	C1402	9.85
SHORT	0.4073	23.0	204.1	29.986	0.45	0.05	C140	5.35
SHORT	0.4073	23.0	204.1	29.986	0.45	0.05	C1402	17.65
SHORT	0.2270	23.0	204.4	29.993	0.25	0.00	C140	9.85
SHORT	0.2270	23.0	204.4	29.993	0.25	0.00	C1402	23.05
SHORT	0.1005	23.0	204.8	29.993	0.20	0.00	C140	23.10
SHORT	0.1005	23.0	204.8	29.993	0.20	0.00	C1402	41.70
LONG	0.8740	22.5	205.1	30.006	2.50	0.10	C140	37.80
LONG	0.8740	22.5	205.1	30.006	2.50	0.10	C1402	42.90
LONG	0.4812	23.4	205.3	30.012	1.50	0.05	C140	72.60
LONG	0.4812	23.4	205.3	30.012	1.50	0.05	C1402	75.60
LONG	0.4556	23.4	204.8	29.938	1.40	0.05	C140	70.20
LONG	0.2840	22.9	205.1	30.021	0.95	0.05	C140	112.80
LONG	0.2840	22.9	205.1	30.021	0.95	0.05	C1402	121.20
LONG	0.1460	23.1	204.9	30.015	0.50	0.00	C140	219.60
LONG	0.1460	23.1	204.9	30.015	0.50	0.00	C1402	240.00
LONG	0.0703	23.4	204.8	29.929	0.30	0.00	C140	459.00
LONG	0.0703	23.4	204.8	29.929	0.30	0.00	C1402	498.00
LONG	0.0703	23.4	204.8	29.929	0.30	0.00	C1402	498.00
LONG	0.0406	23.5	204.9	30.011	0.20	0.00	C140	836.40
LONG	0.0406	23.5	204.9	30.011	0.20	0.00	C1402	939.00

RAW DATA - MIXTURE 7

0.0 % CO

100.0 % CO2

COLUMN	TOTAL FLOW RATE, CC/SEC	TR, DEG C	TC, DEG C	PA, IN HG	PI, PSIG	PO, PSIG	SAMPLE	RET TIME, SEC
SHORT	4.5872	22.8	203.9	30.600	2.85	0.55	C140	0.74
SHORT	4.5872	22.8	203.9	30.600	2.85	0.55	C1402	0.73
SHORT	3.2051	22.8	203.9	30.600	2.00	0.37	C140	0.70
SHORT	3.2051	22.8	203.9	30.600	2.00	0.37	C1402	0.73
SHORT	2.6432	22.8	204.0	30.616	1.70	0.25	C140	1.07
SHORT	2.6432	22.8	204.0	30.616	1.70	0.25	C1402	0.72
SHORT	1.6495	22.9	204.3	30.629	1.10	0.20	C140	1.61
SHORT	1.6495	22.9	204.3	30.629	1.10	0.20	C1402	1.50
SHORT	1.0417	22.8	204.1	30.641	0.70	0.10	C140	2.15
SHORT	1.0417	22.8	204.1	30.641	0.70	0.10	C1402	1.75
SHORT	0.5398	22.8	203.9	30.650	0.45	0.05	C140	5.30
SHORT	0.5398	22.8	203.9	30.650	0.45	0.05	C1402	4.40
SHORT	0.2978	22.6	204.0	30.650	0.30	0.00	C140	8.90
SHORT	0.2978	22.6	204.0	30.650	0.30	0.00	C1402	6.90
SHORT	0.1276	22.6	204.2	30.650	0.20	0.00	C140	27.90
SHORT	0.1276	22.6	204.2	30.650	0.20	0.00	C1402	24.60
LONG	1.0477	22.7	203.8	30.587	2.70	0.10	C140	48.30
LONG	1.0477	22.7	203.8	30.587	2.70	0.10	C140	53.40
LONG	1.0477	22.7	203.8	30.587	2.70	0.10	C1402	42.90
LONG	0.5556	22.8	204.0	30.573	1.50	0.10	C140	102.60
LONG	0.5556	22.8	204.0	30.573	1.50	0.10	C1402	88.20
LONG	0.3066	22.5	203.7	30.587	0.95	0.00	C140	195.60
LONG	0.3066	22.5	203.7	30.587	0.95	0.00	C1402	176.40
LONG	0.1308	22.6	203.7	30.560	0.50	0.00	C140	477.60
LONG	0.1308	22.6	203.7	30.560	0.50	0.00	C1402	451.20
LONG	0.0535	22.3	203.8	30.540	0.25	0.00	C140	1266.00
LONG	0.0535	22.3	203.8	30.540	0.25	0.00	C1402	1245.00

RAW DATA - MIXTURE 1

6.5 % CO

93.5 % CO2

CATALYST ACTIVITY CHECKS

COLUMN	TOTAL FLOW RATE,CC/SEC	TR,DEG C	TC,DEG C	PA, IN HG	PI,PSIG	PO,PSIG	SAMPLE	RET TIME,SEC
LONG	0.3332	22.0	204.0	30.341	1.00	0.05	C140	190.80
LONG	0.3332	22.0	204.0	30.341	1.00	0.05	C140	195.60
LONG	0.3332	22.0	204.0	30.341	1.00	0.05	C1402	176.40
LONG	0.3303	23.3	203.5	30.380	1.00	0.05	C140	171.60
LONG	0.3456	22.1	203.0	30.375	1.00	0.05	C140	164.40
LONG	0.3456	22.1	203.0	30.375	1.00	0.05	C1402	148.80

RAW DATA

CARBON DIOXIDE - HELIUM BINARY MIXTURES

LONG COLUMN

MIXTURE	% CO2	TOTAL FLOW RATE, CC/SEC	TR, DEG C	TC, DEG C	PA, IN HG	PT, PSIG	PD, PSIG	PEAK TIME, SEC
8	7.30	0.2677	23.5	204.4	30.162	0.90	0.05	7035.00
9	26.90	0.2695	23.5	205.1	30.050	0.90	0.05	573.00
10	14.20	0.2586	23.4	203.5	29.814	0.90	0.05	1470.00
11	10.00	0.2646	24.0	205.0	29.770	0.90	0.05	2808.00
12	7.20	0.2454	23.1	205.2	30.003	0.90	0.05	6372.00
13	12.40	0.2308	24.0	206.0	30.002	0.90	0.05	1926.00

RAW DATA

FREE VOLUME DETERMINATIONS

HELIUM CARRIER GAS - ARGON SAMPLE

COLUMN	TOTAL FLOW RATE, CC/SEC	TR, DEG C	TC, DEG C	PA, IN HG	PI, PSIG	PO, PSIG	PEAK TIME, SEC	BYPASS FRACTION
LONG	0.4079	23.8	207.3	30.237	1.50	0.05	36.30	0.232
LONG	0.4079	23.8	207.3	30.237	1.50	0.05	36.20	0.230
LONG	0.4079	23.8	207.3	30.237	1.50	0.05	36.20	0.226
LONG	0.4079	23.8	207.3	30.237	1.50	0.05	36.20	0.223
LONG	0.1975	23.9	207.7	30.230	0.80	0.00	71.40	0.228
LONG	0.1975	23.9	207.7	30.230	0.80	0.00	72.00	0.231
LONG	0.1975	23.9	207.7	30.230	0.80	0.00	72.60	0.231
LONG	0.1255	23.9	207.4	30.226	0.55	0.00	111.00	0.228
LONG	0.1255	23.9	207.4	30.226	0.55	0.00	111.60	0.232
LONG	0.1255	23.9	207.4	30.226	0.55	0.00	111.00	0.229
SHORT	0.4202	23.9	207.4	30.227	0.15	0.00	2.89	
SHORT	0.2556	23.8	206.9	30.223	0.00	0.00	4.65	
SHORT	0.1238	23.7	206.7	30.227	0.00	0.00	9.41	

SHORT COLUMN PEAK TIME VALUES ARE AVERAGE VALUES

APPENDIX H

CALCULATED RESULTS

CALCULATED RESULTS - MIXTURE 1

6.5 % CO

93.5 % CO2

TR,SEC	COLUMN	FLOW RATE,CC/SEC,COLUMN CONDITIONS	PC,MM HG	SAMPLE	G* X 100000.
0.29	SHORT	6.3713	866.1	C140	11.530
0.29	SHORT	6.3713	866.1	C1402	1.294
0.37	SHORT	5.0710	841.5	C140	11.530
0.37	SHORT	5.0710	841.5	C1402	1.854
0.47	SHORT	3.9575	826.4	C140	11.540
0.47	SHORT	3.9575	826.4	C1402	1.600
0.67	SHORT	2.7705	814.3	C140	10.600
0.67	SHORT	2.7705	814.3	C1402	1.133
1.13	SHORT	1.6435	793.8	C140	10.170
1.13	SHORT	1.6435	793.8	C1402	1.583
1.57	SHORT	1.1184	788.6	C140	9.906
1.57	SHORT	1.1184	788.6	C1402	1.395
2.83	SHORT	0.6568	786.0	C140	9.388
2.83	SHORT	0.6568	786.0	C1402	1.735
3.84	SHORT	0.4848	783.5	C140	8.919
3.84	SHORT	0.4848	783.5	C1402	2.007
5.90	SHORT	0.3151	779.6	C140	7.978
5.90	SHORT	0.3151	779.6	C1402	2.731
9.74	SHORT	0.1912	779.7	C140	7.137
9.74	SHORT	0.1912	779.7	C1402	3.156
15.10	SHORT	0.1237	776.0	C140	7.392
15.10	SHORT	0.1237	776.0	C1402	3.409
14.10	LONG	1.1943	852.8	C140	6.073
14.10	LONG	1.1943	852.8	C140	6.001
14.10	LONG	1.1943	852.8	C1402	3.434
23.00	LONG	0.7315	823.1	C140	5.283
23.00	LONG	0.7315	823.1	C1402	4.429
44.20	LONG	0.3811	802.2	C140	5.693
44.20	LONG	0.3811	802.2	C1402	5.258
86.80	LONG	0.1942	788.9	C140	6.348
86.80	LONG	0.1942	788.9	C1402	6.218
171.20	LONG	0.0984	783.1	C140	7.040
171.20	LONG	0.0984	783.1	C1402	7.040

CALCULATED RESULTS - MIXTURE 2

27.6 % CO

72.4 % CO2

TR,SEC	COLUMN	FLOW RATE,CC/SEC,COLUMN CONDITIONS	PC,MM HG	SAMPLE	G* X 100000.
0.20	SHORT	6.3318	850.9	C140	7.169
0.20	SHORT	6.3318	850.9	C1402	1.570
0.29	SHORT	4.4659	824.4	C140	7.725
0.26	SHORT	4.4659	824.4	C1402	0.730
0.33	SHORT	3.7508	814.3	C140	7.918
0.33	SHORT	3.7508	814.3	C1402	1.337
0.50	SHORT	2.5267	799.0	C140	7.500
0.50	SHORT	2.5267	799.0	C1402	1.240
0.78	SHORT	1.6046	786.2	C140	7.246
0.78	SHORT	1.6046	786.2	C1402	0.975
1.12	SHORT	1.1201	778.5	C140	7.378
1.12	SHORT	1.1201	778.5	C1402	1.268
1.80	SHORT	0.6651	797.4	C140	7.487
1.80	SHORT	0.6651	797.4	C1402	1.673
2.54	SHORT	0.4934	773.6	C140	7.011
2.54	SHORT	0.4934	773.6	C1402	1.829
4.17	SHORT	0.3000	769.4	C140	6.718
4.17	SHORT	0.3000	769.4	C1402	2.023
6.87	SHORT	0.1821	770.0	C140	6.585
6.87	SHORT	0.1821	770.0	C1402	3.151
10.30	SHORT	0.1211	768.6	C140	6.743
10.30	SHORT	0.1211	768.6	C1402	4.603
14.70	LONG	1.1500	845.3	C140	6.782
14.70	LONG	1.1500	845.3	C1402	3.428
22.00	LONG	0.7660	820.5	C140	5.469
22.00	LONG	0.7660	820.5	C1402	4.038
44.80	LONG	0.3767	790.2	C140	5.454
44.80	LONG	0.3763	793.3	C140	5.384
44.80	LONG	0.3763	793.3	C1402	5.554
91.80	LONG	0.1836	782.3	C140	6.267
91.80	LONG	0.1836	782.3	C1402	6.513
185.60	LONG	0.0907	773.3	C140	7.215
185.80	LONG	0.0907	773.3	C1402	7.415

CALCULATED RESULTS - MIXTURE 3

63.5 % CO

36.5 % CO2

TR,SEC	COLUMN	FLOW RATE,CC/SEC,COLUMN CONDITIONS	PC,MM HG	SAMPLE	G* X 100000.
0.28	SHORT	6.7364	858.6	C140	3.279
0.28	SHORT	6.7364	858.6	C1402	3.023
0.40	SHORT	4.6651	828.6	C140	3.432
0.40	SHORT	4.6651	828.6	C1402	2.062
0.48	SHORT	3.8988	818.5	C140	2.274
0.48	SHORT	3.8988	818.5	C1402	1.380
0.68	SHORT	2.7403	803.2	C140	3.043
0.68	SHORT	2.7403	803.2	C1402	1.087
1.17	SHORT	1.5987	786.4	C140	2.684
1.17	SHORT	1.5987	786.4	C1402	1.014
2.22	SHORT	0.8388	777.4	C140	2.621
2.22	SHORT	0.8388	777.4	C1402	2.025
3.93	SHORT	0.4727	773.4	C140	2.681
3.93	SHORT	0.4727	773.4	C1402	2.033
8.44	SHORT	0.2206	769.3	C140	2.546
8.44	SHORT	0.2206	769.3	C1402	2.847
18.50	SHORT	0.1004	767.9	C140	2.912
18.50	SHORT	0.1004	767.9	C1402	4.142
14.90	LONG	1.1313	843.2	C140	2.715
14.90	LONG	1.1313	843.2	C1402	2.140
26.80	LONG	0.6299	811.1	C140	2.656
26.80	LONG	0.6299	811.1	C1402	2.656
48.50	LONG	0.3473	790.4	C140	2.627
48.50	LONG	0.3473	790.4	C1402	2.743
94.70	LONG	0.1779	779.8	C140	2.809
94.70	LONG	0.1779	779.8	C1402	3.457
223.20	LONG	0.0755	772.0	C140	6.633
223.20	LONG	0.0755	772.0	C1402	7.561

CALCULATED RESULTS - MIXTURE 4

0.4 % CO

99.6 % CO2

TR,SEC	COLUMN	FLOW RATE,CC/SEC,COLUMN CONDITIONS	PC,MM HG	SAMPLE	G* X 100000.
0.28	SHORT	6.6710	868.5	C140	9.203
0.28	SHORT	6.6710	868.5	C1402	3.876
0.34	SHORT	5.4981	851.7	C140	6.676
0.34	SHORT	5.4981	851.7	C140	10.490
0.34	SHORT	5.4981	851.7	C1402	2.233
0.47	SHORT	3.9741	831.0	C140	2.213
0.47	SHORT	3.9741	831.0	C140	3.144
0.47	SHORT	3.9741	831.0	C1402	2.213
0.47	SHORT	3.9741	831.0	C1402	1.968
0.68	SHORT	2.7330	815.5	C140	2.080
0.68	SHORT	2.7330	815.5	C1402	1.914
0.68	SHORT	2.7330	815.5	C1402	2.014
1.14	SHORT	1.6316	802.5	C140	1.165
1.14	SHORT	1.6316	802.5	C1402	1.611
2.14	SHORT	0.8694	793.5	C140	1.534
2.14	SHORT	0.8694	793.5	C1402	1.555
2.14	SHORT	0.8694	793.5	C1402	1.677
3.78	SHORT	0.4933	788.2	C140	2.823
3.78	SHORT	0.4933	788.2	C1402	2.564
26.10	LONG	0.6459	821.2	C140	3.717
26.10	LONG	0.6459	821.2	C1402	8.555
87.10	LONG	0.1935	793.8	C140	5.060
87.10	LONG	0.1935	793.8	C1402	4.995
45.00	LONG	0.3743	806.1	C140	4.391
45.00	LONG	0.3743	806.1	C1402	4.391
222.00	LONG	0.0761	786.7	C140	5.995
222.00	LONG	0.0761	786.7	C1402	6.114

CALCULATED RESULTS - MIXTURE 5

94.7 % CO

5.3 % CO2

TR,SEC	COLUMN	FLOW RATE,CC/SEC,COLUMN CONDITIONS	PC,MM HG	SAMPLE	G* X 100000.
0.25	SHORT	7.3961	871.9	C140	0.656
0.25	SHORT	7.3961	871.9	C1402	14.340
0.39	SHORT	4.8034	834.4	C140	0.789
0.39	SHORT	4.8034	834.4	C1402	10.900
0.45	SHORT	4.1305	824.0	C140	2.018
0.45	SHORT	4.1305	824.0	C1402	13.680
0.75	SHORT	2.4943	801.8	C140	1.551
0.75	SHORT	2.4943	801.8	C1402	11.900
1.28	SHORT	1.4512	790.3	C140	1.863
1.28	SHORT	1.4512	790.3	C1402	11.220
2.06	SHORT	0.9055	784.3	C140	1.752
2.06	SHORT	0.9055	784.3	C1402	10.750
2.06	SHORT	0.9055	784.3	C1402	11.130
4.15	SHORT	0.4478	779.2	C140	1.988
4.15	SHORT	0.4478	779.2	C1402	7.852
6.76	SHORT	0.2749	774.8	C140	2.598
6.76	SHORT	0.2749	774.8	C1402	6.572
27.20	LONG	0.6198	814.3	C140	2.003
27.20	LONG	0.6198	814.3	C1402	2.398
49.10	LONG	0.3436	794.6	C140	1.945
49.10	LONG	0.3436	794.6	C1402	2.372
103.90	LONG	0.1627	780.5	C140	2.015
103.90	LONG	0.1627	780.5	C1402	2.376
191.30	LONG	0.0883	778.7	C140	2.217
191.30	LONG	0.0883	778.7	C1402	2.462

CALCULATED RESULTS - MIXTURE 6

100.0 % CO

0.0 % CO2

TR,SEC	COLUMN	FLOW RATE,CC/SEC,COLUMN CONDITIONS	PC,MM HG	SAMPLE	G* X 100000.
0.46	SHORT	4.0290	817.1	C140	1.991
0.46	SHORT	4.0290	817.1	C1402	53.770
0.55	SHORT	3.3928	808.2	C140	1.469
0.55	SHORT	3.3928	808.2	C1402	21.530
0.92	SHORT	2.0396	790.0	C140	1.572
0.92	SHORT	2.0396	790.0	C1402	26.790
1.52	SHORT	1.2272	778.5	C140	1.776
1.52	SHORT	1.2272	778.5	C1402	11.800
2.96	SHORT	0.6276	774.6	C140	1.719
2.96	SHORT	0.6276	774.6	C1402	10.580
5.27	SHORT	0.3529	768.3	C140	1.839
5.27	SHORT	0.3529	768.3	C1402	7.141
11.90	SHORT	0.1566	767.0	C140	1.996
11.90	SHORT	0.1566	767.0	C1402	5.303
17.30	LONG	0.9747	829.4	C140	1.961
17.30	LONG	0.9747	829.4	C1402	2.449
30.50	LONG	0.5525	802.4	C140	2.207
30.50	LONG	0.5525	802.4	C1402	2.364
32.20	LONG	0.5242	797.9	C140	1.884
50.60	LONG	0.3327	788.4	C140	1.928
50.60	LONG	0.3327	788.4	C1402	2.189
97.20	LONG	0.1736	775.3	C140	1.952
97.20	LONG	0.1736	775.3	C1402	2.278
201.00	LONG	0.0840	768.0	C140	1.973
201.00	LONG	0.0840	768.0	C1402	2.271
346.00	LONG	0.0487	767.5	C140	2.167
346.00	LONG	0.0487	767.5	C1402	2.620

CALCULATED RESULTS - MIXTURE 7

0.0 % CO

100.0 % CO2

TR,SEC	COLUMN	FLOW RATE,CC/SEC,COLUMN CONDITIONS	PC,MM HG	SAMPLE	G* X 100000.
0.29	SHORT	5.4643	865.2	C140	3.751
0.29	SHORT	5.4643	865.2	C1402	3.668
0.40	SHORT	4.6601	838.5	C140	1.743
0.40	SHORT	4.6601	838.5	C1402	1.917
0.48	SHORT	3.8950	828.1	C140	2.833
0.48	SHORT	3.8950	828.1	C1402	1.159
0.75	SHORT	2.4811	811.6	C140	2.567
0.75	SHORT	2.4811	811.6	C1402	2.239
1.17	SHORT	1.5924	799.0	C140	1.852
1.17	SHORT	1.5924	799.0	C1402	1.098
2.23	SHORT	0.8330	791.4	C140	2.998
2.23	SHORT	0.8330	791.4	C1402	2.118
4.02	SHORT	0.4631	786.3	C140	2.636
4.02	SHORT	0.4631	786.3	C1402	1.557
9.34	SHORT	0.1992	783.8	C140	4.294
9.34	SHORT	0.1992	783.8	C1402	3.531
14.60	LONG	1.1594	849.3	C140	3.943
14.60	LONG	1.1594	849.3	C140	4.538
14.60	LONG	1.1594	849.3	C1402	3.312
26.50	LONG	0.6381	817.9	C140	4.713
26.50	LONG	0.6381	817.9	C1402	3.823
46.90	LONG	0.3599	801.5	C140	5.089
46.90	LONG	0.3599	801.5	C1402	4.432
108.40	LONG	0.1557	789.2	C140	5.382
108.40	LONG	0.1557	789.2	C1402	4.998
262.50	LONG	0.0643	782.2	C140	5.989
262.50	LONG	0.0643	782.2	C1402	5.864

CALCULATED RESULTS - MIXTURE 1

6.5 % CO

93.5 % CO2

CATALYST ACTIVITY CHECKS

TR,SEC	COLUMN	FLOW RATE,CC/SEC,COLUMN CONDITIONS	PC,MM HG	SAMPLE	G* X 100000.
43.10	LONG	0.3908	797.8	C140	5.458
43.10	LONG	0.3908	797.8	C140	5.635
43.10	LONG	0.3908	797.8	C1402	4.926
43.10	LONG	0.3915	798.8	C140	4.770
41.90	LONG	0.4043	798.7	C140	4.708
41.90	LONG	0.4043	798.7	C1402	4.109

CALCULATED RESULTS

CARBON DIOXIDE - HELIUM BINARY MIXTURES

LONG COLUMN

MIXTURE	% CO2	FLOW RATE, CC/SEC, COLUMN CONDITIONS	G* X 10000.
8	7.3	0.3128	20.450
9	28.9	0.3153	1.520
10	14.2	0.3016	3.950
11	10.0	0.3085	7.840
12	7.2	0.2878	16.890
13	12.4	0.2698	4.660

CALCULATED RESULTS

FREE VOLUME DETERMINATIONS

HELIUM CARRIER GAS - ARGON SAMPLE

COLUMN	FLOW RATE, CC/SEC, COLUMN CONDITIONS	COLUMN FREE VOLUME, CC
LONG	0.4697	17.05
LONG	0.4697	17.00
LONG	0.4697	17.00
LONG	0.4697	17.00
LONG	0.2331	16.64
LONG	0.2331	16.78
LONG	0.2331	16.92
LONG	0.1493	16.57
LONG	0.1493	16.66
LONG	0.1493	16.57
SHORT	0.6567	1.90
SHORT	0.4013	1.87
SHORT	0.1944	1.83

APPENDIX I

FORTRAN PROGRAM FOR COLUMN SIMULATION

```
C      W.D.SMITH, COLUMN SIMULATION PROGRAM
       DIMENSION X(500),Y(500),XA(500),YB(500),XB(500),YC(500)
 1000  READ(5,10) DT,EPS,XT,YT,N,M
   10  FORMAT(4F10.0,2I5)
       READ(5,11) XI,YI,IX,IY
   11  FORMAT(2F10.0,2I5)
       READ(5,12) EK1,EK2,EK3,EK4,AZ,BZ
   12  FORMAT(6F10.0)
       READ(5,13) RK1,RK2,RK3,RK4
   13  FORMAT(4F10.0)
       READ(5,14) TM1,TM2,TM3,TM4,TM5
   14  FORMAT(5F10.0)
       READ(5,17) CZ,EK5,RK5
   17  FORMAT(3F10.0)
       WRITE(6,15) XT,N,AZ,BZ,EK1,EK2,EK3,EK4,RK1,RK2,RK3,RK4
   15  FORMAT(39H1   W.D.SMITH, COLUMN SIMULATION PROGRAM//
      119H CO MOLE FRACTION =,F6.3,4H N =,I5,5H AZ =,F6.3,5H BZ =,F6.3/
      26H EK1 =,F8.4,6H EK2 =,F8.4,6H EK3 =,F8.4,6H RK4 =,F8.4/
      36H RK1 =,F8.4,6H RK2 =,F8.4,6H RK3 =,F8.4,6H RK4 =,F8.4)
       WRITE(6,18) CZ,EK5,RK5
   18  FORMAT(5H CZ =,F8.5,6H EK5 =,F8.5,6H RK5 =,F8.6)
       WRITE(6,16) XI,YI
   16  FORMAT(5H0XI =,F8.4,5H YI =,F8.4)
       DO 20 I=1,500
       X(I)=0.
       Y(I)=0.
       XA(I)=0.
       YB(I)=0.
       YC(I)=0.
   20  XB(I)=0.
       IXPRN=0
       MIN=M
       IZ=0
       MTM=0
       MFAC=1
       MUL=1
       TFAC=1.
       A=AZ/(1.+EK1*XT)
       B=BZ/(1.+EK2*XT+EK3*YT*(1.+EK4/(EK2*XT)))
       C=CZ/(1.+EK5*YT)
       ZB=EK3*YT*B*EK4/(EK2*XT)
       F1=EK1*A
       F2=EK2*B
       F3=EK3*B
       F4=EK4*B/ZB
       F5=EK5*C
       WRITE(6,25) F1,F2,F3,F4,A,B,ZB
   25  FORMAT(5H0F1 =,F8.4,4H F2=,F8.4,5H F3 =,F8.4,5H F4 =,F8.4/
```

```
   14H A =,F8.4,4H B =,F8.4,5H ZB =,F8.4)
    WRITE(6,26) F5,C
 26 FORMAT(5H F5 =,F8.5,4H C =,F8.5)
100 DELT=DT*TFAC
    RT1=RK1*DELT*A
    RT2=RK2*DELT*B
    RT3=RK3*DELT*B
    RT4=RK4*DELT*B
    RT5=RK5*DELT*C
    T1=(2.-DELT)/(2.+DELT)
    T2=2./(2.+DELT)
    T3=DELT/(2.+DELT)
    MTM=MTM+MFAC
    TCNT=MTM
    TIME=TCNT*DT
    XF=0.
    YF=0.
    IF(MTM.GT.IX) GO TO 110
    XF=2.*XI
110 IF(MTM.GT.IY) GO TO 115
    YF=2.*YI
115 I=IZ
    IS=IZ+1
200 I=I+1
    XO=X(I)
    YO=Y(I)
    XAO=XA(I)
    XBO=XB(I)
    YBO=YB(I)
    YCO=YC(I)
    R1=RT1*(XO-XAO/F1)
    R2=RT2*(XO-XBO/F2)
    R3=RT3*(YO-YBO/F3)
    R4=RT4*(YBO-XBO/F4)
    R5=RT5*(YO-YCO/F5)
    XA(I)=XAO+R1
    XB(I)=XBO+R2+R4
    YB(I)=YBO+R3-R4
    YC(I)=YCO+R5
    XN=XO*T1+XF*T3-T2*(R1+R2)
    YN=YO*T1+YF*T3-T2*(R3+R5)
    XF=XN+XO
    YF=YN+YO
    X(I)=XN
    Y(I)=YN
    IF(I.GE.N) GO TO 300
    IF(XN.GT.EPS) GO TO 200
    XN=0.
```

```
      IF(YN.GT.EPS) GO TO 200
      YN=0.
      IF(I.GT.IS) GO TO 210
      IZ=IS
      IF(IZ.GE.N) GO TO 501
      GO TO 200
  210 IF(I.LT.MIN) GO TO 200
      MIN=I
  300 IF(TIME.LT.(TM1-EPS)) GO TO 400
      MFAC=2
      TFAC=2.0
      IF(TIME.LT.(TM2-EPS)) GO TO 400
      MFAC=5
      TFAC=5.0
  400 TMUL=MUL
      TPRN=TMUL*TM3-EPS
      XPRN=IXPRN
      IF(TIME.LT.(XPRN*TM5)) GO TO 410
      IXPRN=IXPRN+1
      WRITE(6,402) (X(I),I=1,60)
      WRITE(6,402) (Y(I),I=1,60)
      WRITE(6,402) (XA(I),I=1,60)
      WRITE(6,402) (XB(I),I=1,60)
      WRITE(6,402) (YB(I),I=1,60)
      WRITE(6,402) (YC(I),I=1,60)
  402 FORMAT(1H0/(1H ,10F10.6))
  410 IF(TIME.LT.TPRN) GO TO 500
      MUL=MUL+1
      XL=X(N)
      YL=Y(N)
      XY=XL+YL
      WRITE(6,401) TIME,XL,YL,XY
  401 FORMAT(8H  TIME =,F6.2,6H  XL =,F8.5,6H  YL =,F8.5,7H XL+YL=,
     1F8.5)
  500 IF(TIME.LT.TM4) GO TO 100
      READ(5,510) IEND
  510 FORMAT(I2)
      IF(IEND.GT.0) GO TO 1000
  501 CALL EXIT
      END
```

BIBLIOGRAPHY

1. Amberg, C. H., and Seanor, D. A., Proc. Int. Congr. Catal. 3rd, 450 (1965).

2. Aris, R., Proc. Roy. Soc. A235, 67 (1956).

3. Bank, C. A., and Verdurmen, E. A. Th., J. Inorg. and Nucl. Chem. 25, 667 (1963).

4. Barrere, C. A., and Deans, H. A., AIChE J. 14, 280 (1968).

5. Beeck, O., Smith, A. E., and Wheeler, A., Proc. Roy. Soc. A177, 62 (1940).

6. Catalyst Handbook, Springer-Verlag, New York (1970).

7. Cha, D. Y., and Parravano, G., J. Catalysis 11, 228 (1968).

8. Collins, C. G., and Deans, H. A., AIChE J. 14, 25 (1968).

9. Deans, H. A., Horn, F. J. M., and Klauser, G., AIChE J. 16, 426 (1970).

10. Deans, H. A., and Lapidus, L., AIChE J. 6, 656 (1960).

11. Eberly, P. E., Jr., J. Phys. Chem. 65, 68 (1961).

12. Ehrlich, G., J. Chem. Phys. 34, 39 (1961).

13. Eischens, R. P., and Webb, A. N., J. Phys. Chem. 20, 1048 (1952).

14. Emmett, P. H., Sabatier, P., and Reid, E. E., Catalysis Then and Now, Franklin Publishing Co., Englewood, N. J. (1965).

15. Ertl, G., Surface Science 7, 309 (1967).

16. Gangwal, S. K., Hudgins, R. R., Bryson, A. W., and Silveston, P. L., "Interpretation of Chromatographic Peaks by Fourier Analysis," presented at the 3rd Joint Meeting of the AIChE and the Puerto Rican Institute of Chemical Engineers, San Juan, P. R., 1970.

17. Garner, W. E., J. Chem. Soc., 1239 (1947).

18. Garner, W. E., and Veal, F. J., J. Chem. Soc., 1487 (1935).

19. Giddings, J. C., J. Chromatography 3, 443 (1960).

20. Giddings, J. C., and Keller, R., J. Chromatography 3, 205 (1960).

21. Giddings, J. C., and Seager, S. L., I&EC Fundamentals 1, 277 (1962).

22. Grubner, O., Advances in Chromatography 6, 173 (1968).

23. Hayward, D. O., and Gomer, R. J., J. Chem. Phys. 30, 1617 (1959).

24. Hayward, D. O., and Trapnell, B. M. W., Chemisorption, 2nd ed., Butterworth, London (1964).

25. James, A. T., and Martin, A. J. P., Biochem. J. 50, 679 (1952).

26. Juvet, R. S., Jr., and Dal Nogare, S., Anal. Chem. 36, 36R (1964).

27. Keulemans, A. I. M., Gas Chromatography, 2nd ed., Reinhold Publishing Corp., New York (1959).

28. Klinkenberg, A., Chem. Eng. Sci. 15, 255 (1961).

29. Kobayashi, R., Chappelear, P. S., and Deans, H. A., Ind. Eng. Chem. 59, 63 (1967).

30. Koonce, K. T., Deans, H. A., and Kobayashi, R., AIChE J. 11, 259 (1965).

31. Kubin, M., Coll. Czech. Chem. Comm. 30, 2900 (1965).

32. Kubokawa, Y., Bull. Chem. Soc. Japan 33, 555 (1960).

33. Kucera, E., J. Chromatography 19, 277 (1965).

34. Langon, M. A. H., and Trapnell, B. M. W., Proc. Roy. Soc. A227, 387 (1955).

35. Littlewood, A. B., Phillips, C. S. G., and Price, D. T., J. Chem. Soc., 1480 (1955).

36. Martin, A. J. P., Analyst 81, 52 (1956).

37. Martin, A. J. P., and Synge, R. L. M., Biochem. J. 35, 1358 (1941).

38. Musser, G. S., Ph.D. Thesis, Rice University (1965).

39. Nekipelov, V. N., and Kasatkina, L. A., Kinetika i Kataliz (Eng. Transl.) 11, 910 (1970).

40. Norris, T. H., and Ruben, S., J. Chem. Phys. 18, 1595 (1950).

41. Padberg, G., and Smith, J. M., J. Catalysis 12, 172 (1968).

42. Purnell, H., Gas Chromatography, Wiley and Sons, Inc., New York (1962).

43. Schneider, P., and Smith, J. M., AIChE J. 14, 762 (1968).

44. Schneider, P., and Smith, J. M., AIChE J. 14, 886 (1968).

45. Stalkup, F. I., and Deans, H. A., AIChE J. 9, 106 (1963).

46. Stalkup, F. I., and Kobayashi, R., AIChE J. 9, 121 (1963).

47. Stalkup, F. I., and Kobayashi, R., J. Chem. Eng. Data 8, 546 (1963).

48. Stroeva, S. S., Kulkova, N. V., and Temkin, M. E., Doklady Akad. Nauk. S.S.S.R. 124, 628 (1959).

49. Suzuki, M., and Smith, J. M., J. Catalysis 21, 336 (1971).

50. Taylor, G., Proc. Roy. Soc. A219, 186 (1953).

51. Taylor, J. H., and Amberg, C. H., Can. J. Chem. 39, 535 (1961).

52. Titani, T., Kiyoura, T., and Adachi, A., Bull. Chem. Soc. Japan 38, 2075 (1965).

53. Tswett, M., Ber. Deut. Botan. Ges. 24, 316 (1906).

54. Uchida, H., Oba, M., Isogai, N., and Hasegawa, T., Bull. Chem. Soc. Japan 41, 479 (1968).

55. Van Deemter, J. J., Zuiderweg, F. J., and Klinkenberg, A., Chem. Eng. Sci. 5, 271 (1956).

56. Winter, E. R. S., Advances in Catalysis 10, 196 (1958).

57. Wydeven, T., and Leban, M., J. Chrom. Sci. 7, 445 (1969).

58. Yoneda, Y., Makishima, S., and Hirasa, K., J. Am. Chem. Soc. 80, 4503 (1958).